Article

Cell Reports

Mammalian cells use the autophagy process to restrict avian influenza virus replication

Graphical abstract

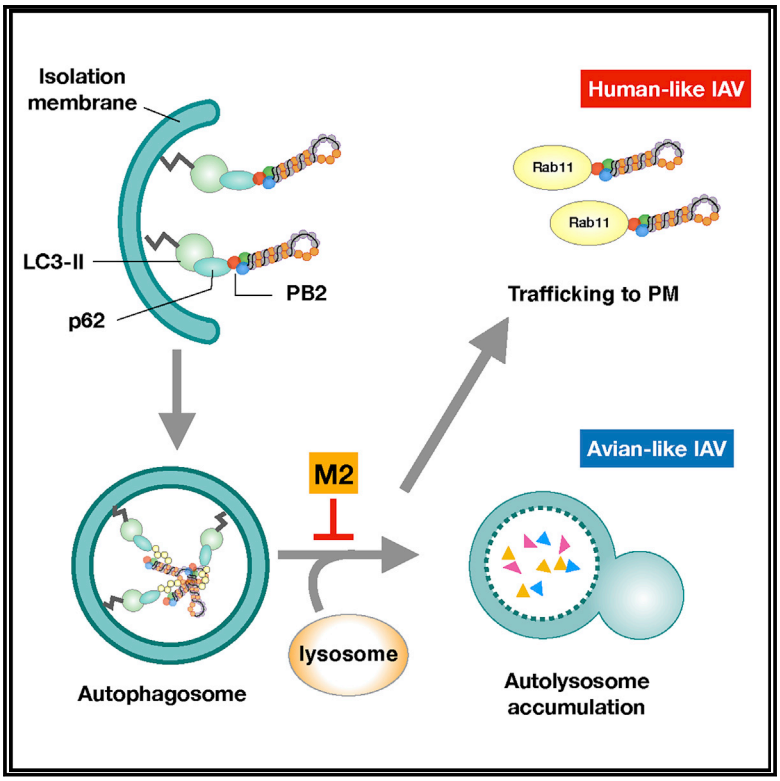

Authors

Siwen Liu, Bobo Wing-Yee Mok, Shaofeng Deng, ..., Yixin Chen, Kwok-Yung Yuen, Honglin Chen

Correspondence

hlchen@hku.hk

In brief

Liu et al. find that influenza A virus vRNP with avian-PB2 forms aggregates in mammalian cells and induces the accumulation of autolysosome, due to increased autophagic flux. They further identify that autophagy receptor p62/SQSTM1 targets newly synthesized vRNPs to form autophagosome through viral polymerase protein PB2 during influenza virus infection.

Highlights

- vRNP aggregates form in mammalian cells infected with avian influenza A virus (IAV)
- Autophagy process is involved in the formation of vRNP aggregates
- Avian-like IAV induces higher autophagic flux and more autolysosome accumulation
- p62/SQSTM1 targets vRNP through interaction with viral PB2

Liu et al., 2021, Cell Reports *35*, 109213
June 8, 2021
https://doi.org/10.1016/j.celrep.2021.109213

CellPress

Cell Reports

CellPress
OPEN ACCESS

Article

Mammalian cells use the autophagy process to restrict avian influenza virus replication

Siwen Liu,[1] Bobo Wing-Yee Mok,[1] Shaofeng Deng,[1] Honglian Liu,[1] Pui Wang,[1] Wenjun Song,[1,4] Pin Chen,[1] Xiaofeng Huang,[1] Min Zheng,[1] Siu-Ying Lau,[1] Conor J. Cremin,[1] Chun-Yee Tam,[1] Baiying Li,[2] Liwen Jiang,[2] Yixin Chen,[3] Kwok-Yung Yuen,[1] and Honglin Chen[1,5,*]

[1]State Key Laboratory for Emerging Infectious Diseases, InnoHK Centre for Virology, Vaccinology, and Therapeutics, and Department of Microbiology, Li Ka Shing Faculty of Medicine, The University of Hong Kong, Hong Kong SAR, China

[2]School of Life Sciences, Centre for Cell & Developmental Biology and State Key Laboratory of Agrobiotechnology, The Chinese University of Hong Kong, Hong Kong SAR, China

[3]National Institute of Diagnostics and Vaccine Development in Infectious Diseases, and State Key Laboratory of Molecular Vaccinology and Molecular Diagnostics, School of Public Health, Xiamen University, Xiamen 361005, China

[4]State Key Laboratory of Respiratory Disease, Institute of Integration of Traditional and Western Medicine, Guangzhou Medical University, Guangzhou 510180, China

[5]Lead contact

*Correspondence: hlchen@hku.hk

https://doi.org/10.1016/j.celrep.2021.109213

SUMMARY

Host adaptive mutations in the influenza A virus (IAV) PB2 protein are critical for human infection, but their molecular action is not well understood. We observe that when IAV containing avian PB2 infects mammalian cells, viral ribonucleoprotein (vRNP) aggregates that localize to the microtubule-organizing center (MTOC) are formed. These vRNP aggregates resemble LC3B-associated autophagosome structures, with aggresome-like properties, in that they cause the re-distribution of vimentin. However, electron microscopy reveals that these aggregates represent an accumulation of autophagic vacuoles. Compared to mammalian-PB2 virus, avian-PB2 virus induces higher autophagic flux in infected cells, indicating an increased rate of autophagosomes containing avian vRNPs fusing with lysosomes. We found that p62 is essential for the formation of vRNP aggregates and that the Raptor-interacting region of p62 is required for interaction with vRNPs through the PB2 polymerase subunit. Selective autophagic sequestration during late-stage virus replication is thus an additional strategy for host restriction of avian-PB2 IAV.

INTRODUCTION

Host barriers serve to restrict cross-species infections. However, some avian influenza viruses have evolved multiple host-adaptive strategies, including the ability to infect mammalian hosts and achieve cross-species transmission. Pandemic influenza is caused by efficient cross-species transmission of a novel subtype of influenza virus, arising either through reassortment or direct host adaptation processes (Taubenberger and Kash, 2010). Host-adaptive mutations have been identified in viral functions associated with different stages of the influenza virus life cycle, including receptor binding for cell entry, viral genome replication, and late-stage viral genome trafficking for virion packaging (Cauldwell et al., 2014; Schrauwen and Fouchier, 2014). While switching of receptor-binding specificity to the new host will ultimately determine the efficiency of cross-species transmission, adaptation of viral polymerase for replication in a novel host could occur first, thereby priming the virus for a cross-species jump (de Graaf and Fouchier, 2014; Wang et al., 2019). Adaptive mutations in the viral replication complex are thought to be important for preparing a virus for the evolution or acquisition of other mutations that promote cross-species infection (Huang et al., 2017; Wang et al., 2019). Multiple adaptation markers in the polymerase subunits, nucleoprotein, and non-structural proteins have been identified in various influenza viruses causing human infections. Among all known host-adaptive substitutions, mutations in the PB2 subunit are the most commonly found and extensively studied (Huang et al., 2017; Mänz et al., 2012; Mehle and Doudna, 2009; Naffakh et al., 2008; Soh et al., 2019; Song et al., 2014; Subbarao et al., 1993; Yamada et al., 2010).

Influenza virus uses the viral polymerase complex, which is composed of PB1, PB2, and PA subunits, to replicate and transcribe the viral genome in the cell nucleus. Various influenza virus subtypes containing polymerases with host-adaptive mutations such as E627K, D701N, K526R, or G590S/Q591R (H1N1) display higher polymerase activity in mammalian cells than viruses with polymerases lacking adaptive mutations (Gabriel et al., 2005; Mehle and Doudna, 2009; Song et al., 2014). Some of these characterized mutations are associated with human infections caused by H5 and H7 subtype avian influenza viruses (Chen et al., 2006b; Hatta et al., 2001; Song et al., 2014). However, details of the molecular basis for the promotion of cross-species virus replication in mammalian cells by these adaptive mutations

remains largely unknown. Acquiring the positively charged E627K substitution may facilitate PB2 interaction with viral nucleoprotein (NP) in the ribonucleoprotein (RNP) polymerase complex, enhancing viral polymerase activity in mammalian cells (Gabriel et al., 2005; Labadie et al., 2007; Naffakh et al., 2008). The host protein, ANP32A, has recently been found to play a role in restricting virus replication in mammalian cells through differential regulation of the activity of viral polymerases carrying PB2-627K (human) or PB2-627E (avian) signatures (Domingues and Hale, 2017; Long et al., 2016, 2019). The effect of PB2 host-adaptive mutations is not limited to the enhancement of viral polymerase activity. Interaction with host machinery is integral to the export of the viral genome to the cytoplasm for packaging into new virions that bud from the membrane of infected cells (Lakdawala et al., 2016). Host-adaptation mutations in PB2 have also been observed to affect viral interactions with host nuclear import machinery (Boivin and Hart, 2011; Gabriel et al., 2008; Pumroy et al., 2015). Retinoic acid-inducible gene-I (RIG-I) plays an important role in antiviral immunity and functions as a sensor of RNA viruses, binding to the influenza virus nucleocapsid to directly inhibit virus infection in a manner independent of interferon induction (Weber et al., 2015). The segmented viral genome structure allows influenza viruses to consolidate optimal replication fitness within different genome constellations through reassortment and adaptive mutations. Host restrictions act on different stages of the virus life cycle, and influenza viruses have evolved with multiple layers of adaptive strategies to evade these restrictions. Selective autophagy has been shown to play an important role in innate and acquired immunity, facilitating the capture and clearance of incoming pathogens; however, influenza viruses have evolved not only to evade this host restriction but also to hijack the autophagy process to facilitate virus replication (Ding et al., 2014; Levine, 2005).

To explore other mechanisms underlying the host restriction of avian influenza virus replication in mammalian cells, and in particular those occurring after nuclear export of the newly synthesized viral genome, we analyzed intracellular trafficking of viral RNP (vRNP) in influenza virus-infected cells. We found that influenza viruses carrying avian-type PB2 consistently form vRNP aggregates in infected cells, while viruses carrying mammalian-type PB2, regardless of the type of mutation, do not form such aggregates. We further demonstrated that these vRNP aggregates are closely associated with the autophagic process. Human influenza viruses have evolved to subvert host restriction by autophagy to promote virus replication, and it seems that one of the adaptive strategies associated with PB2 may involve evasion of the antiviral effects of the cellular autophagy process during intracellular trafficking of viral genomes to the assembly site for packaging. Our data show that influenza viruses carrying avian-type PB2 evade autophagic inhibition less effectively than those with human-type PB2, leading to lower replication efficiency. Different mechanisms lead to the autophagy process in cells. We identified p62/SQSTM1, an important cargo receptor for autophagy (Bjørkøy et al., 2005; Pankiv et al., 2007), as critical for the formation of vRNP aggregates in cells infected with viruses bearing avian-type PB2, leading to autophagy-related host restriction of avian influenza virus replication in mammalian cells.

RESULTS

Aggregates of vRNP accumulate in mammalian cells infected with influenza virus containing avian PB2

The H7N9 virus has caused more human infections than any other subtype of avian influenza virus since its 2013 emergence in China (Chen et al., 2013; Wang et al., 2017). We have speculated that the 2013 H7N9 virus uses multiple host adaptive strategies to cause human infections (Huang et al., 2017; Song et al., 2014). To explore the molecular mechanism of mammalian adaptation for avian influenza viruses, we examined cellular trafficking of vRNA using combined RNA fluorescence *in situ* hybridization (FISH) and immunofluorescence analysis. The 2013 H7N9 virus is a reasssortant virus containing internal genes from circulating avian H9N2 and hemagglutinin (HA) and neuraminidase (NA) genes from influenza viruses present in wild birds (Gao et al., 2013). In this experiment, vRNA probes for the specific recognition of PB2 from H9N2 or NP from WSN were used. Notably, we found that cells infected with avian H9N2 virus display distinct large vRNA aggregates and that these colocalize with Rab11 in the perinuclear area (Figure 1A). Similar vRNA aggregates were not observed during infection with a mammalian cell-adapted virus, A/WSN/33. Interestingly, vRNA aggregates containing WSN NP genome segments were observed in WSN and H9N2 virus co-infected cells; these co-localized with H9N2 PB2 segments, suggesting that formation of vRNP aggregates is dictated by the presence of avian PB2. To understand which viral component from H9N2 virus contributes to the presence of vRNA aggregates, we tested two viruses, one containing RNP genes (PA, PB1, PB2, and NP) derived from an H7N9 virus isolated from a human case (Song et al., 2014) and the other containing RNP genes from the avian H9N2 virus, which provided the internal genes of the 2013 H7N9 virus, with the remaining genome segments of each virus being derived from the WSN strain. The infection of A549 cells showed that only cells infected with virus containing avian H9N2 RNP, but not RNP derived from the H7N9 human virus, produced vRNP aggregates (Figure 1B). We then tested a panel of reassortant WSN viruses with human-origin H7N9 RNPs containing PB2 with various adaptive mutations or individual RNP components derived from an avian-origin H7N9 strain. No vRNP aggregates were observed in cells infected with viruses containing known PB2 adaptive mutations or viruses containing avian-type PB1, PA, or NP. However, vRNP aggregates were observed in cells infected with reassortant virus containing avian-type PB2 (Figure 1C; Table S1). Growth analysis revealed that RNPs containing avian-type PB2 cause attenuation of viral growth rate in A549 cells (Figure S1). To facilitate subsequent experiments analyzing the contribution of avian-type PB2 to the accumulation of vRNA aggregates in mammalian cells, we constructed a reassortant WSN virus in which the PB2 was mutated from 627K (wild type [WT]) to 627E to create an avian-type PB2 (Figure S2A). This pair of viruses, which differ only in the 627 residues (WSN-WT and WSN-627E), were examined, confirming that A549 cells infected with WSN-627E but not WSN-WT develop vRNA aggregates, which became apparent from 8 h post-infection (Figure 1D). To further validate this difference between influenza viruses containing either 627K or 627E PB2, we infected normal human

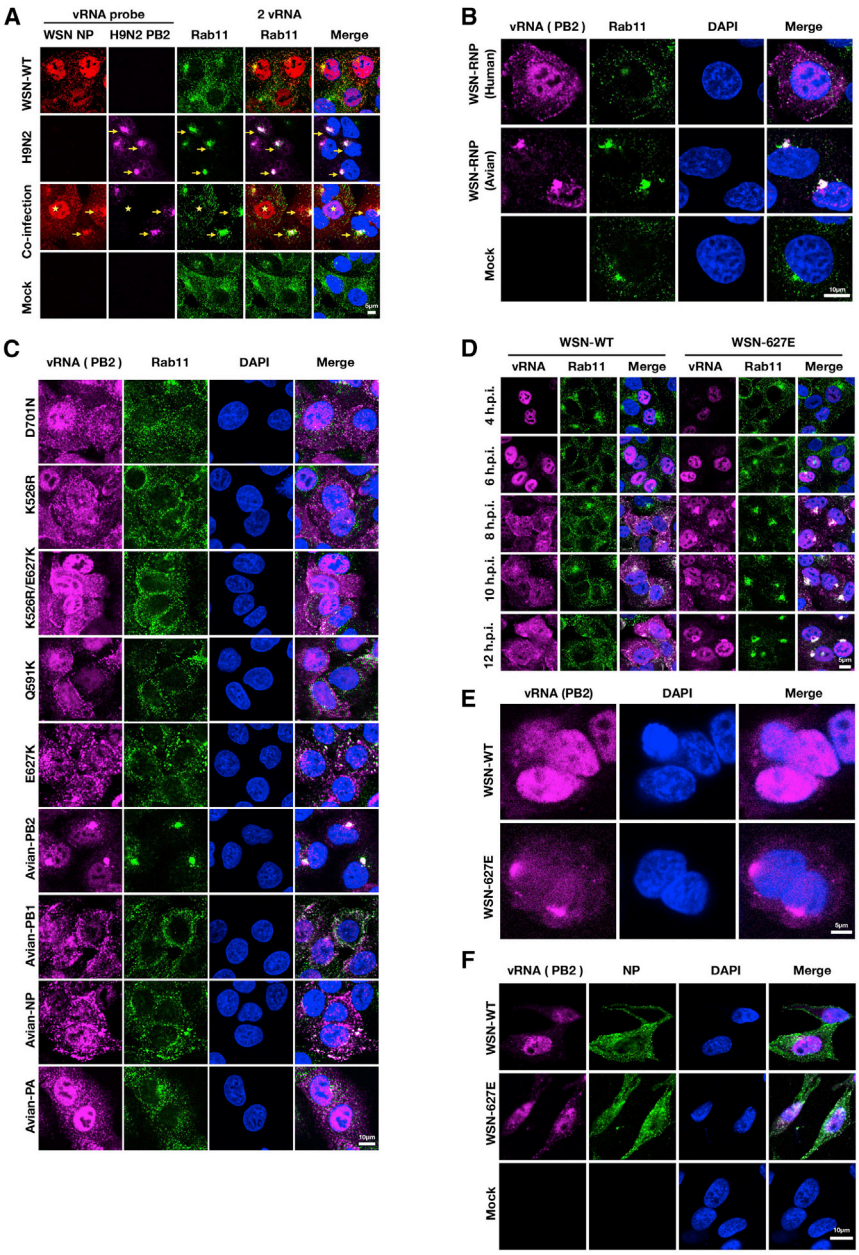

Figure 1. Accumulation of vRNA aggregates in mammalian cells infected with influenza virus containing avian PB2

A549 cells were mock infected or infected with the indicated viruses at an MOI of 5. At 10 hpi (hours post-infection), cells were fixed and combined RNA FISH and immunofluorescence analysis was performed.

(A) Infection with WSN or avian H9N2 virus or co-infection with WSN and avian H9N2 viruses. FISH staining with NP vRNA probe derived from WSN (shown in red) or PB2 vRNA probe derived from avian H9N2 (shown in purple) and immunofluorescence staining for endogenous Rab11 (shown in green) are shown. vRNA aggregates that co-localized with endogenous Rab11 are labeled with arrows. For co-infection, the cell infected only with the WSN strain is labeled with a star. NP (WSN) vRNA and PB2 (H9N2) vRNA probes were used to differentiate viral RNP complexes in cells co-infected with both viruses.

(B) Infection with WSN-RNP (human) or WSN-RNP (avian) viruses, with FISH staining using PB2 vRNA probes derived from WSN or H9N2 strains, respectively, and antibody staining of endogenous Rab11 (green).

(C) A549 cells were infected with the indicated reassortant viruses and stained using PB2 vRNA probe (purple) and endogenous Rab11-specific antibody (green).

(D) A549 cells were infected with the indicated reassortant viruses and combined FISH and immunofluorescence staining performed at different time points with PB2 vRNA probe (purple) and endogenous Rab11-specific antibody (green).

(E) NHBE primary cells were infected with WSN-WT or WSN-627E viruses at an MOI of 5. Cells were fixed at 10 hpi and stained with PB2 vRNA probe (purple).

(F) DF-1 cells were mock infected or infected with WSN-WT or WSN-627E viruses at an MOI of 5. Cells were fixed at 10 hpi and stained using PB2 vRNA probe (purple) and antibody specific for the viral NP protein (green).

Merge images also include DAPI staining (blue). Images were acquired by confocal LSM 780 microscopy. Scale bars (5 or 10 μm) are displayed at the bottom right of each panel. All of the results are representative of 3 independent experiments.

bronchial epithelial (NHBE) primary cells with WSN-WT or WSN-627E and examined them using PB2-specific vRNA probes. Similar to the observation in A549 cells, vRNA aggregates were observed in WSN-627E but not in WSN-627K-infected NHBE cells (Figure 1E). In contrast, infection of DF-1 avian cells with either WSN-WT or WSN-627E virus does not produce vRNA aggregates (Figure 1F), suggesting that formation of vRNA aggregates only occurs in mammalian cells infected with virus containing avian-type PB2. Growth rate analysis also revealed that WSN-WT replicates to a higher level in A549 cells than WSN-627E, but there is no apparent difference between WSN-WT and WSN-627E virus replication in infected DF-1 cells (Figure S2B). WSN-WT virus also induces a higher level of expression of the host cytokine gene IFIT1 in A549 cells than WSN-627E, while there is no apparent difference in cytotoxicity between the two viruses (Figures S2C and S2D). Examination with a probe recognizing viral mRNA showed that viral mRNA does not associate with aggregates (Figure S2E). It has been reported that influenza virus containing PB2-627E is prone to increased RIG-I recognition (Weber et al., 2015). However, we observed no apparent effect of RIG-I knockout (KO) on the accumulation of vRNA aggregates in A549 cells infected with WSN-627E or WSN-WT virus, although RIG-I KO did increase the growth of WSN-WT, but not WSN-627E virus (Figure S3). These

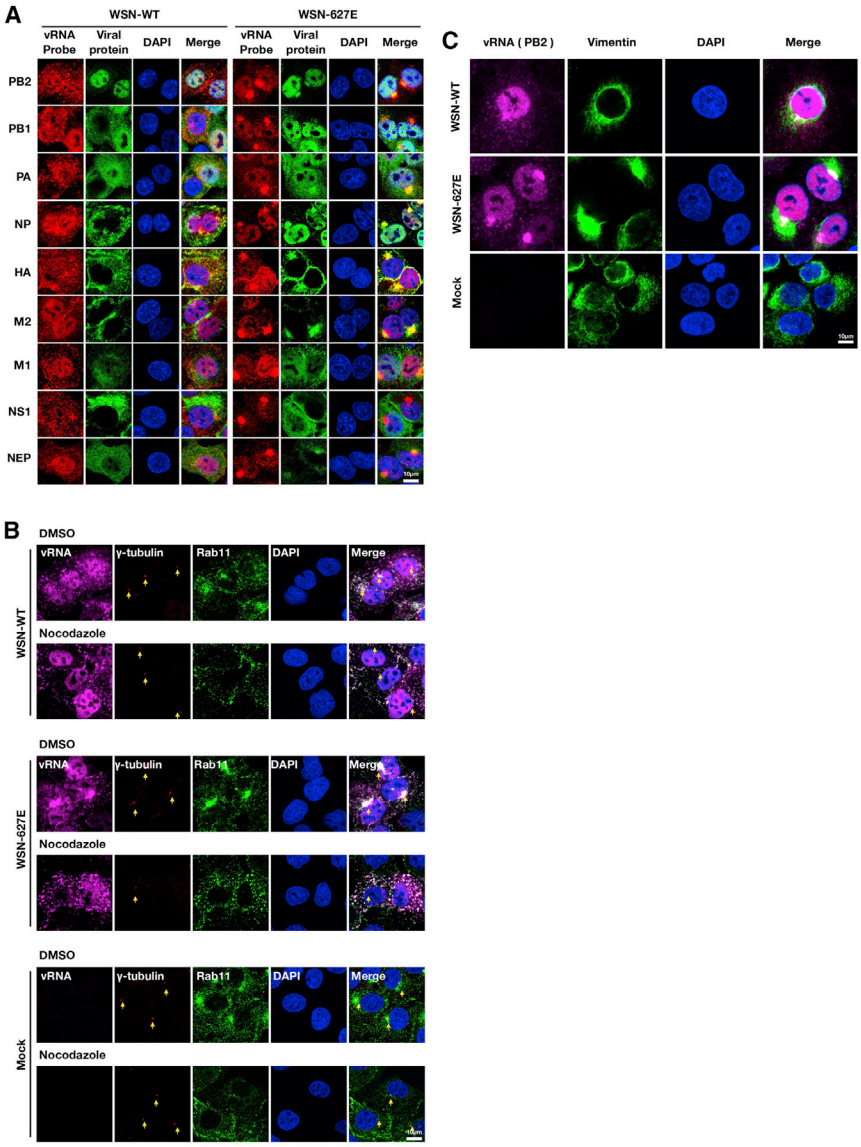

Figure 2. Characterization of vRNA aggregates in WSN-627E virus-infected cells

(A) A549 cells were infected with WSN-WT or WSN-627E viruses at an MOI of 5 for 10 h and cells processed for FISH and IFA assays using PB2 vRNA probe (red) and antibodies specific for the indicated viral proteins (green), respectively.

(B) A549 cells were mock infected or infected with WSN-WT or WSN-627E viruses at an MOI of 5. At 4 hpi, 10 μM nocodazole or DMSO (solvent control) was added to cells. Cells were fixed at 10 hpi, and combined RNA FISH and immunofluorescence staining with vRNA probe (purple) and antibodies against endogenous γ-tubulin (red) and Rab11 (green) was performed.

(C) A549 cells were mock infected or infected with WSN-WT or WSN-627E virus at an MOI of 5. Cells were fixed at 10 hpi and FISH assay staining with vRNA probe (purple) and immunofluorescence staining with antibody against endogenous vimentin protein (green) was performed.

Merge images also include DAPI staining (blue). Images were acquired by confocal LSM 780 microscopy. Scale bars (10 μm) are included on each panel. Results are representative of 3 independent experiments.

results reveal a mechanism of host restriction involving the accumulation of vRNP aggregates during avian virus replication in mammalian cells; these vRNP aggregates occur exclusively in the presence of avian-type PB2, with the acquisition of mammalian adaptive mutations preventing vRNA accumulation.

Characterization of vRNP aggregates in WSN-627E virus-infected cells

To understand the molecular properties of the vRNA aggregates observed above and investigate whether aggregated vRNAs are stalled at a checkpoint in the usual virion assembly process, we examined the co-localization of viral proteins with vRNP in infected cells. While a previous report using mass spectrometry showed that the non-structural protein (NS1) may be included in the virion (Hutchinson et al., 2014), it is understood that normally viral polymerases (PB1, PB2, and PA), which combine with vRNA and NP to form the RNP complex, together with M1, M2, HA, and NA are required for the packaging of new virions during virus replication (Lamb and Krug, 2001). The staining of viral proteins by immunofluorescence and vRNA by RNA FISH showed that vRNP aggregates co-localize with NP, polymerases, and other structural proteins, but not with NS1 (Figure 2A), indicating that these aggregates contain all of the components of the viral RNP complex, not only viral RNA. Upon nucleocytoplasmic export, vRNAs are subject to intracellular trafficking to the plasma membrane for packaging and budding (Amorim et al., 2011). Nuclear exported vRNPs have been reported to accumulate transiently around microtubule organizing centers (MTOCs) before being further transported to packaging sites via a microtubule and Rab11-dependent mechanism (Eisfeld et al., 2011; Momose et al., 2007). We examined whether the vRNP aggregates associate with MTOC and found that in PB2-627E virus-infected A549 cells, they co-localize with Rab11 and γ-tubulin, and that treatment with nocodazole to interfere with microtubule polymerization leads to the disassociation of vRNA aggregates (De Brabander et al., 1976) (Figure 2B). These results suggest that the accumulation of vRNP aggregates is related to the intercellular trafficking process occurring after nuclear export. The endocytic recycling compartment (ERC)/trans-Golgi system and endoplasmic reticulum (ER) are involved in the assembly and packaging processes during influenza virus replication (de Castro Martin et al., 2017; Guichard et al., 2014). Co-staining using

the Golgi markers TGN46 (*trans*-Golgi) and GM130 (*cis*-Golgi) showed vRNP aggregates localized in the vicinity of the Golgi apparatus and rearrangement of Golgi complexes, compared to those in mock infected cells (Figure S4A). We found that vRNP aggregates are not associated with calnexin, a chaperone that assists in protein folding and quality control in the ER apparatus (Figure S4A). Vimentin, the major component of the cytoskeleton, is important for anchoring organelles in the cytosol and has been shown to eliminate toxic proteins (Johnston et al., 1998; Ogrodnik et al., 2014; Rujano et al., 2006). It is notable that the presence of vRNP aggregates in WSN-627E virus-infected cells is associated with the displacement of vimentin, whereas this effect was not observed with WSN-WT virus (Figure 2C). We observed that vRNP aggregates appear to be wrapped by vimentin, and suspect that this action may be related to the eventual removal of aggregates. Another study showed that an autophagy-associated protein, TUFM, interacts with the PB2 of influenza virus (Kuo et al., 2017). However, we found that TUFM is not associated with vRNP aggregates in WSN-627E virus-infected cells (Figure S4B), suggesting that TUFM may be involved in another host restriction mechanism during avian influenza virus replication. These data suggest that the accumulation of vRNP aggregates is associated with the intracellular trafficking process during influenza virus replication and that the observed vRNA aggregates appear to exhibit aggresome-like properties.

WSN-627E-induced vRNP aggregates are associated with the autophagy process

We then investigated whether these vRNP aggregates are involved in the autophagy process, since previous studies have reported that influenza viruses hijack the autophagy process to facilitate virus replication (Beale et al., 2014; Gannagé et al., 2009; Yeganeh et al., 2018). We reasoned that the accumulation of vRNP aggregates during virus replication may be caused by a difference in the interaction between RNPs containing PB2-627K or PB2-627E, with the host autophagy process following nucleocytoplasmic export. Combined vRNA FISH and immunofluorescence assays showed that the autophagosome marker LC3B over-accumulates within and co-localizes with vRNP aggregates in WSN-627E virus-infected cells, but that this pattern is not observed in WSN-WT virus-infected cells (Figure 3A). Previous studies on the autophagy-related protein Atg5 suggested that the Atg12-Atg5/Atg16 complex helps to form the autophagosome membrane (Chen and Zhong, 2012; Eskelinen, 2008). Antibody staining for endogenous Atg5 showed partial co-localization of vRNA aggregates with Atg5 in cells infected with WSN-627E virus (Figure 3B), suggesting that Atg5 also contributes to vRNA aggregate formation. Upon autophagy induction, the cytoplasmic form of LC3, LC3-I, is conjugated with phosphatidylethanolamine (PE) to form LC3-II and recruited to the isolation membrane for the elongation and maturation of autophagosomes (Kabeya et al., 2004). The amount of LC3-II is a conventional indicator for the number of autophagosomes and autophagy-related structures (Kabeya et al., 2000). Consistent with previous studies (Beale et al., 2014; Gannagé et al., 2009), the levels of LC3-II increased in influenza virus-infected cells along the course of virus replication and RNP nuclear export (Figure 3C, left panel). It should be noted that levels of the M2 protein, which is required for blocking the fusion of autophagosomes with lysosomes to disrupt the autophagy process during virus replication, are significantly lower in WSN-627E virus-infected cells, while levels of NP, PB1, and PB2 are not apparently affected. Quantitative analysis of LC3-II to actin ratios in both WSN-WT and WSN-627E virus-infected cells indicates that the accumulation of autophagosomes in WSN-WT infected cells is significantly higher than in WSN-627E virus-infected cells at the late stage of infection (Figure 3C, right panel). To further investigate the mechanisms underlying the accumulation of autophagosomes induced by influenza virus infection, we used transmission electron microscopy (TEM) to visualize autophagic structures in WSN-WT and WSN-627E virus-infected cells. In uninfected cells, autophagic structures (autophagosomes and autolysosomes) were rarely observed. In contrast, upon BafA1 (bafilomycin A1, a V-ATPase inhibitor and inhibitor of lysosome degradation) treatment, large autolysosomes enclosed by a single membrane were observed in mock-infected cells, due to the effect of BafA1 in blocking the degradation of autolysosomes, thereby causing the accumulation of autophagic substrates in autolysosomes (Figure 3D). In A549 cells infected with WSN-WT virus, there were significantly increased numbers of phagophores (structures with isolation or sequestration membranes) and autophagosomes (structures with completed double membranes), suggesting the continuous formation and accumulation of autophagosomes. In contrast, more autolysosomes than autophagosomes were observed in cells infected with WSN-627E. Moreover, cells infected with WSN-627E virus showed an obvious increase in the numbers of autolysosomes following treatment with BafA1, suggesting an increased autophagic flux in cells infected with WSN-627E compared to those infected with WSN-WT virus. While these results confirm that influenza virus infection induces the formation of autophagosomes, our data further suggest that vRNAs of WSN-627E virus are driven to degradation through the autolysosomal process in a more aggressive way than those of WSN-627K virus in infected cells.

Infection with virus containing PB2-627E induces higher autophagic flux

The accumulation of autophagosomes is a balance between autophagosome biogenesis and autophagosome degradation by lysosomes (Mizushima et al., 2010). We hypothesize that mammalian cells respond differently to infection with influenza viruses containing either PB2-627K or PB2-627E, leading to distinct effects on viral replication. To confirm this, we used the tandem mRFP/mCherry-EGFP-LC3 reporter system to monitor the autophagic flux in virus-infected cells (Kimura et al., 2007). Due to the differential pH stability of red and green fluorescent proteins, the fluorescent signal of EGFP is quenched by the low pH environment inside lysosomes, whereas the fluorescence of mRFP/mCherry remains stable. Therefore, EGFP and mRFP/mCherry double-positive (yellow) dots correspond to autophagosomes before fusion, while after fusion with lysosomes only mRFP/mCherry single-positive (red) dots are left (Figure 4A). In our experiment, mammalian A549 cells were transfected with mRFP/mCherry-EGFP-LC3 (ptfLC3) and then infected with virus. Combined vRNA FISH and immunofluorescence assays showed that in cells infected with

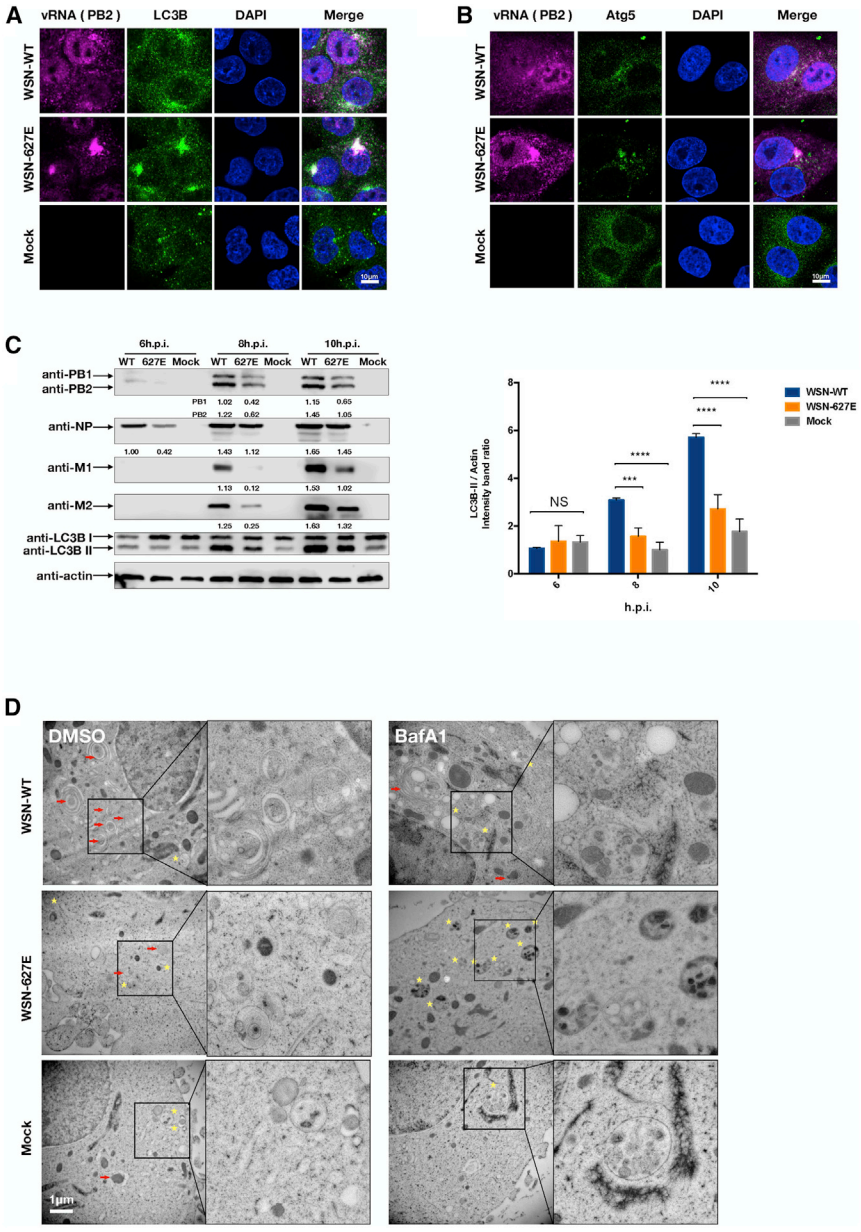

Figure 3. vRNA aggregates in WSN-672E virus infected cells are associated with the autophagy process

(A) A549 cells were mock infected or infected with the indicated reassortant viruses at an MOI of 5. At 10 hpi, cells were processed for combined RNA FISH and immunofluorescence assay by staining with PB2 vRNA probe (purple) and endogenous LC3-specific antibody (green). Scale bar, 10 μm. Images are representative of 3 independent experiments.

(B) A549 cells were mock infected or infected with WSN-WT or WSN-627E viruses at an MOI of 5. Cells were fixed at 10 hpi and combined RNA FISH and immunofluorescence staining with vRNA probe (purple) and antibodies against endogenous Atg5 (green) was performed. Merge images also include DAPI staining (blue). Images were acquired by confocal LSM 780 microscopy. Scale bar, 10 μm. Images are representative of 3 independent experiments.

(C) Confluent HEK293T cells were mock infected or infected with WSN-WT or WSN-627E at an MOI of 2. Cells were collected at 6, 8, and 10 hpi and whole-cell lysates analyzed for the expression of PB1, PB2, NP, M1, M2, LC3, and actin (loading control) by western blot using specific antibodies. Ratios of LC3-II to actin band intensity at the different time points were calculated, based on the results of 3 independent experiments. Mean values are displayed, and error bars represent standard deviations (SDs). Statistical significance was analyzed by 1-way analysis of variance: ***$p < 0.001$, ****$p < 0.0001$, NS, not significant.

(D) A549 cells were mock infected or infected with the indicated reassortant viruses for 4 h at an MOI of 5, then treated with DMSO (solvent control) or 100 nM BafA1 for 6 h. Cells were fixed via high-pressure freezing, followed by freeze substitution, and observed under transmission electron microscopy. Boxes within areas are shown enlarged on the right of each pair of electron micrograph images. Developing and mature autophagosomes (red arrows) and autolysosomes (yellow stars) are indicated. Scale bar, 1 μm.

WSN-WT virus, both mRFP/mCherry and EGFP are observed, indicating that mature autophagosomes have not fused with lysosomes (Figure 4B). However, only the red fluorescence of mRFP/mCherry is seen in cells infected with WSN-627E virus, where the avian-type PB2 induces formation of vRNP aggregates; presumably the EGFP has been quenched by the low pH inside autolysosomes following the fusion of autophagosomes and lysosomes, indicating that the autophagy process is complete.

To quantitatively measure the level of autophagic flux, murine embryonic fibroblast (MEF) cells stably expressing mRFP/mCherry-EGFP-LC3 fusion protein were infected with WSN-WT or WSN-627E virus, treated or untreated with BafA1 and subjected to flow cytometry analysis of EGFP to mCherry ratios. The ratio of EGFP to mCherry is used as an indicator to quantify the autophagic flux level, with a higher ratio of EGFP to mCherry representing lower autophagic flux. Compared to mock-infected and positive-control Earle's balanced salt solution (EBSS)-starved cells, the ratio of EGFP:mCherry in both WSN-WT and WSN-627E infected cells is higher, indicating that influenza virus infection triggers autophagosome formation (Figure 4C). However, the ratio of EGFP:mCherry is significantly higher in cells infected with WSN-WT than in those infected with WSN-627E virus, indicating the upregulation of degradation events in autolysosomes in WSN-627E virus-infected cells. BafA1 works by inhibiting autophagosome, lysosome, and autolysosome acidification, therefore treatment with BafA1 decreases EGFP-LC3 degradation in virus-infected cells. To further verify that the accumulation of vRNP aggregates is caused by a failure to subvert the autophagy process to

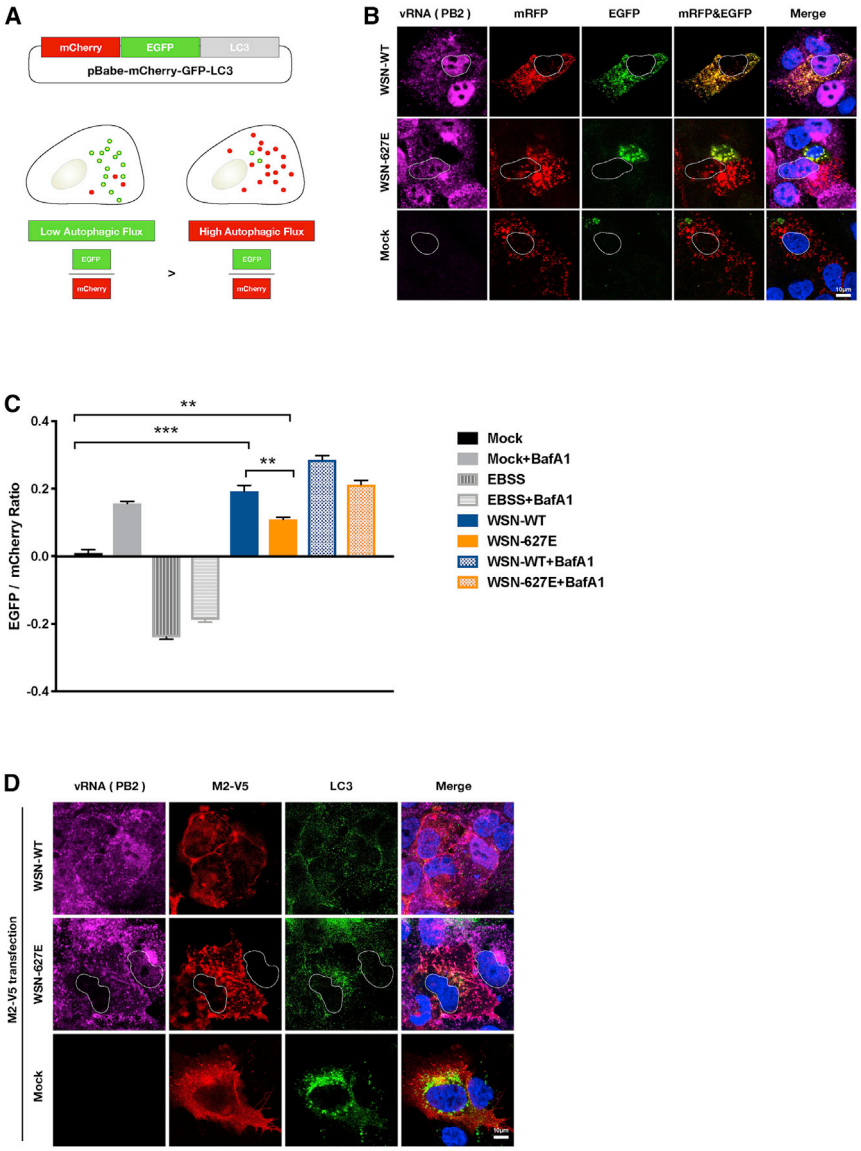

Figure 4. PB2-627E containing virus induces higher autophagic flux activity

(A) Illustration of MEF cell line stably expressing mRFP/mCherry-EGFP-LC3 and a representation of different levels of autophagic flux. Due to differential sensitivity to pH changes, when fusion of autophagosomes with lysosomes decreases the pH in the vesicle, EGFP is degraded, but not mCherry.

(B) A549 cells were first transfected with a ptfLC3 plasmid encoding the mRFP/mCherry-EGFP-LC3 fusion protein for 36 h and then mock infected or infected with the indicated reverse genetic versions of viruses. At 8 hpi, cells were fixed, FISH stained with PB2 vRNA probe (purple), and analyzed by confocal fluorescence microscopy. Images are representative of 3 independent experiments.

(C) The MEF mRFP/mCherry-EGFP-LC3 stable cell line was mock infected or infected with WSN-WT or WSN-627E virus at an MOI of 2 for 16 h and cells then processed for flow cytometry analysis. EBSS (Earle's balanced salt solution) was used to induce autophagy in positive control cultures. Cells were treated with BafA1 as in the procedure described above. Data are presented as means ± SDs (n = 3). Statistical significance was analyzed by 1-way analysis of variance: $^{**}p < 0.01$ and $^{***}p < 0.001$.

(D) A549 cells were transfected with a plasmid for expression of M2 tagged with V5 for 36 h and then mock infected or infected with the indicated reverse genetic versions of viruses. Cells were stained with PB2 vRNA probe (purple), α-V5 antibody (red), and α-LC3 antibody (green) and analyzed by fluorescence microscopy.

Merge images also include DAPI staining (blue). Images were acquired by confocal LSM 780 microscopy. Scale bars, 10 μm. Results shown are representative of 3 independent experiments.

promote virus assembly, we used ectopic expression of M2 to block the autophagic flux in WSN virus-infected cells. In WSN-WT virus-infected cells, no apparent vRNP aggregates were observed and LC3 was evenly distributed in the cytoplasm (Figure 4D). It is notable that in the WSN-627E virus-infected cells, vRNP aggregates disappeared only in cells expressing M2-V5. While previous studies have reported different mechanisms associated with influenza virus PB2 host adaptation, the current data suggest a formerly uncharacterized mechanism for host restriction of viruses containing avian-type PB2 through selective autophagic degradation of vRNP during virus replication.

The p62 cellular protein targets vRNP to the autophagosome

We have shown that mammalian cells respond differently to infection by influenza viruses carrying human or avian PB2 polymerases, demonstrated by the selective formation of vRNP aggregates, presumably through an altered autophagic process that promotes the degradation of vRNAs from viruses containing avian-type PB2. Consequently, a greater proportion of avian-type virus vRNAs are directed to the autophagosome degradation pathway than vRNA complexes of mammalian-adapted viruses carrying PB2-627K. Since autophagy is required for human-type influenza virus replication, it would be interesting to understand how this selective degradation is initiated depending on whether the influenza virus has avian- or mammalian-type PB2. Since the host factor p62 has been reported to mediate delivery of autophagic substrates for degradation through selective autophagy (Komatsu et al., 2010; Rogov et al., 2014), we tested whether p62 may be involved in the formation of influenza vRNP aggregates containing avian-type PB2. Blocking the fusion of autophagosomes with lysosomes leads to the accumulation of p62 in the autophagy pathway (Pankiv et al., 2007). Confirming this, we observed an obvious speckled pattern of p62 accumulation in BafA1-treated cells and co-localization of vRNP aggregates

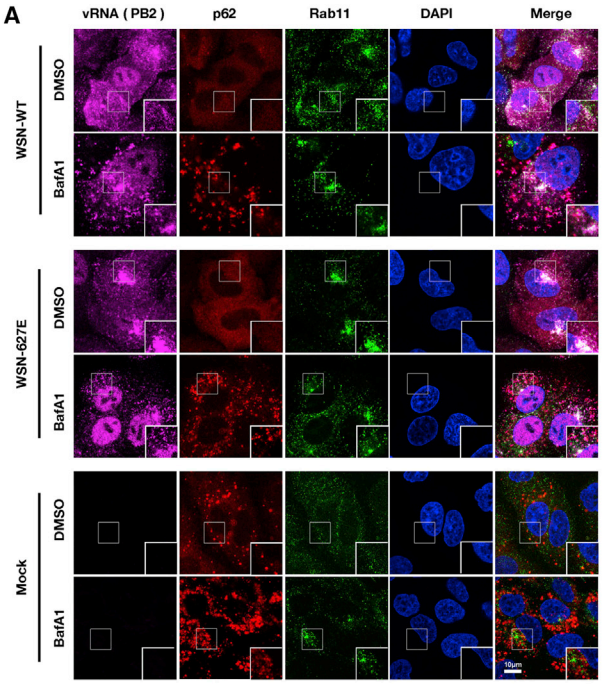

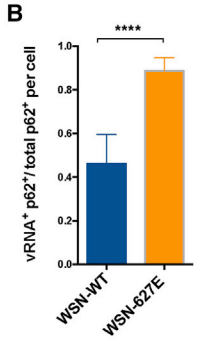

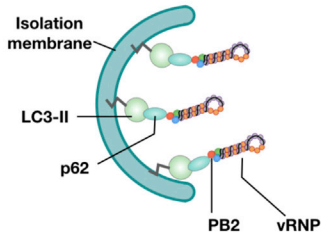

Figure 5. vRNP is targeted to autophagosomes through the cargo receptor p62

(A) A549 cells were mock infected or infected with the indicated reassortant viruses at an MOI of 5. Cells were treated with DMSO (solvent control) or BafA1 (100 nM) at 4 hpi, fixed at 10 hpi, and then FISH staining for PB2 vRNA (purple) and immunofluorescence staining for endogenous Rab11 (green) and endogenous p62 (red) performed. Merge images also include DAPI staining (blue). Images were acquired by confocal LSM 780 microscopy. Scale bar, 10 μm. Images are representative of 3 independent experiments.

(B) Quantification of vRNA and p62 double-positive dots in 30 BafA1-treated A549 cells infected with either WSN-WT or WSN-627E virus. Data are presented as means ± SDs (n = 3). Statistical significance was analyzed by 1-way analysis of variance: ****$p < 0.0001$.

(C) Proposed role of p62 in targeting influenza virus vRNP complexes to the autophagosome.

and Rab11 in untreated WSN-627E-infected cells, and diminished vRNP aggregates in WSN-PB2-627E virus-infected cells treated with BafA1 (Figure 5A). Staining with LAMP1 showed that lysosomes were more concentrated in the areas where vRNP aggregates localized in WSN-PB2-627E virus-infected cells (Figures S5A and S5B), supporting the contention that vRNP aggregates are associated with the autolysosome degradation process. The quantification of vRNA and p62 double-positive dots revealed a significantly higher occurrence of co-localization of vRNA and p62 in WSN-627E virus-infected cells, compared to those infected with WSN-WT (Figure 5B). However, no co-localization of another autophagy receptor, optineurin (OPTN), and vRNA aggregates was observed (Figure S5C). A possible role for p62 in mediating the direction of influenza virus vRNP to the autophagic process is proposed (Figure 5C). Co-immunoprecipitation (coIP) of vRNP complexes (PB1, PB2, PA, and NP) with FLAG-tagged p62 showed interaction between vRNPs and p62, with PB2-627E vRNPs demonstrating a higher level of interaction than PB2-627K vRNPs (Figure 6A). To determine which component of vRNPs interacts with p62, coIP assays were performed and showed no clear interaction between p62 and individual PB1, PA, or NP proteins (Figure 6B). The p62 protein contains multiple domains and serves as a hub for several signaling pathways (Katsuragi et al., 2015). To further define which regions of p62 are essential for interaction with viral PB2, a series of truncated p62 constructs (Figure 6C) were generated and subjected to immune co-precipitation assays with PB2-627K or -627E. As expected, both PB2-627K and -627E interact with full-length p62. Interestingly, PB2 still interacts with C-terminal truncated p62, which lacks ubiquitin-associated (UBA) domain, PEST, LC3 interacting region (LIR), and the tumor necrosis factor receptor-associated factor 6 (TRAF6) domain (D2) and all intermediary C-terminal truncated versions of p62 (D3–D6). However, the N-terminal region of p62, containing only the PB1 domain (D1), does not interact with PB2 protein (Figure 6C), suggesting that viral PB2 proteins interact with p62 through the region containing the ZZ domain (amino acid [aa] residues 128–225). Further analysis showed that the region of p62 that is between the ZZ and TRAF6 domains (residues 163–225) is involved in the interaction between viral PB2 proteins and p62 (Figures S6B and S6C).

Having established that vRNP complexes are involved in the autophagic process during infection through the association of viral PB2 and p62 protein, we sought to determine whether the host protein p62 plays a role in the formation of vRNA aggregates during WSN-627E infection. We examined multiple lines of virus-infected p62 KO A549 cells for vRNA aggregates. Notably, vRNA

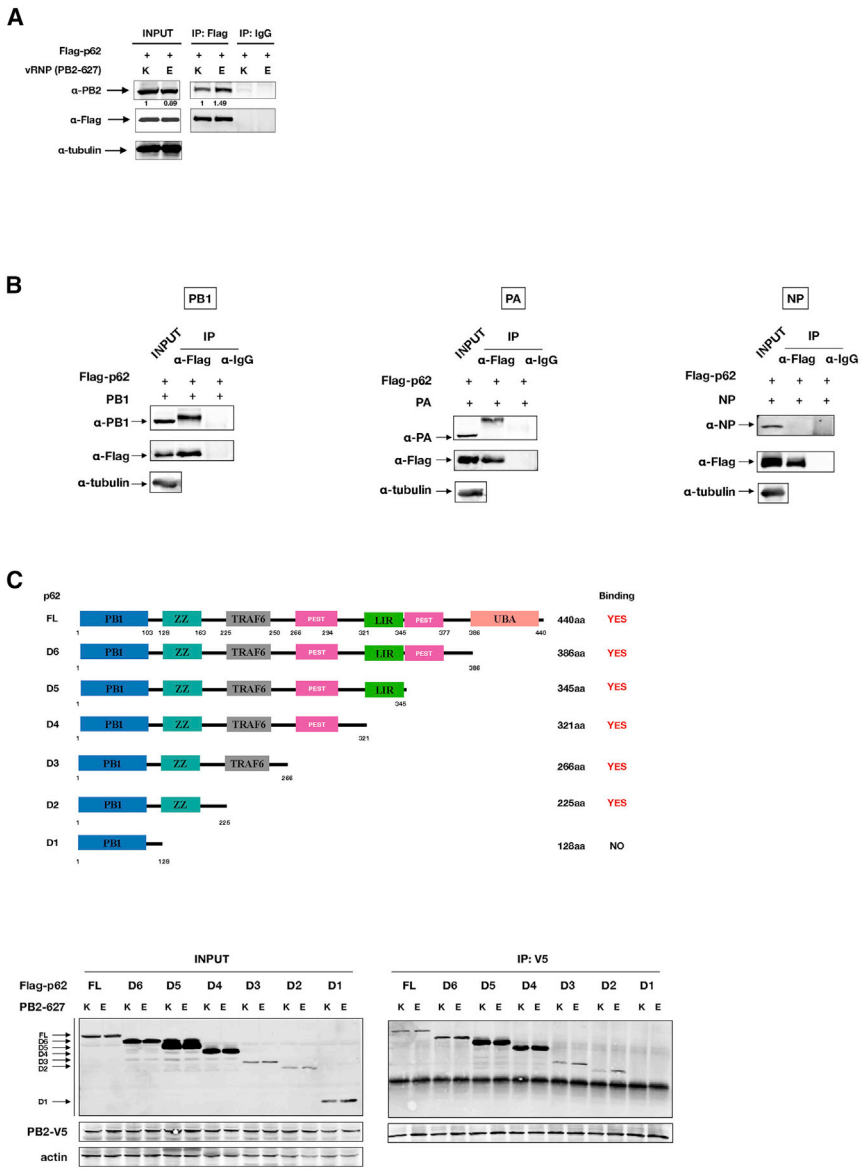

Figure 6. p62 interacts with vRNP through the viral PB2 protein

(A) HEK293T cells were co-transfected with vRNP complex components derived from WSN-627K or -627E viruses and FLAG-tagged p62. Whole-cell lysates were used for immunoprecipitation (IP) with α-FLAG, followed by immunoblotting with α-FLAG (for p62), α-PB2, and α-tubulin.

(B) HEK293T cells were co-transfected with PB1, PA, or NP alone, plus FLAG-tagged p62. Whole-cell lysates were used for IP with α-FLAG, followed by immunoblotting with α-FLAG (for p62), α-PB1, α-PA, α-NP, and tubulin.

(C) Illustration of p62 functional domains and p62 mutant proteins with progressively large C-terminal deletions (D1–D6) (upper panel). HEK293T cells were co-transfected with plasmids encoding progressively deleted FLAG-tagged p62 mutants, as indicated, and V5-tagged PB2 proteins derived from WSN-WT or WSN-627E viruses. Whole-cell lysates were used for IP with α-V5, followed by immunoblotting with α-FLAG (for p62), α-V5 (for viral PB2), and actin (lower panel).

Results shown are representative of 3 independent experiments.

aggregates were not observed in any of the different clones of A549-p62-KO cells infected with WSN-627E virus (Figure 7A), suggesting that the formation of vRNA aggregates in WSN-627E influenza virus infections is p62 dependent. In addition, it was shown that the ectopic expression of p62 by transfection restored vRNP aggregate formation in p62-KO cells infected with WSN-627E virus, while the expression of p62 with deletion of residues 163–225 did not have such an effect (Figure S6A). We reasoned that formation of vRNP aggregates in WSN-627E virus-infected mammalian cells must affect virus replication efficiency. We further examined the effect of p62 KO on influenza virus replication and found that the depletion of p62 significantly enhances the replication of WSN-627E virus, but has only a limited effect on WSN-WT virus (Figure 7B). However, the KO of p62 had no apparent effect on the polymerase activity of PB2-WT or PB2-627E (Figure 7C). These results reveal a host restriction strategy targeting avian-type influenza virus PB2 following nucleocytoplasmic export and support a mechanism associated with early events in the autophagic process, mediated through p62, that interferes with vRNP intracellular trafficking and promotes the formation of autolysosomes to sequester vRNPs of influenza viruses containing avian polymerase PB2; host adaptive mutations in PB2 allow influenza viruses to evade such restriction (Figure 7D).

DISCUSSION

Influenza virus is one of the few RNA viruses that transcribes and replicates its genome in the nucleus. Nucleocytoplasmic export and trafficking of synthesized vRNA to the cytoplasmic site for virion packaging are critical steps in the life cycle of influenza virus and may be subject to host restriction. Influenza viruses have evolved with the ability to use the cellular autophagy process to facilitate viral replication and budding through inhibition of autophagic degradation by the viral M2 protein (Beale et al., 2014; Gannagé et al., 2009). It is noted that these studies have used human influenza viruses that have fully adapted to replicate in human cells. Here, we reveal a mechanism in which mammalian cells respond differently to infection with avian- and mammalian-type PB2-bearing influenza viruses, restricting intracellular trafficking of avian-type PB2 virus through the formation of vRNA aggregates following nuclear export. Multiple adaptive substitutions have been identified in the PB2

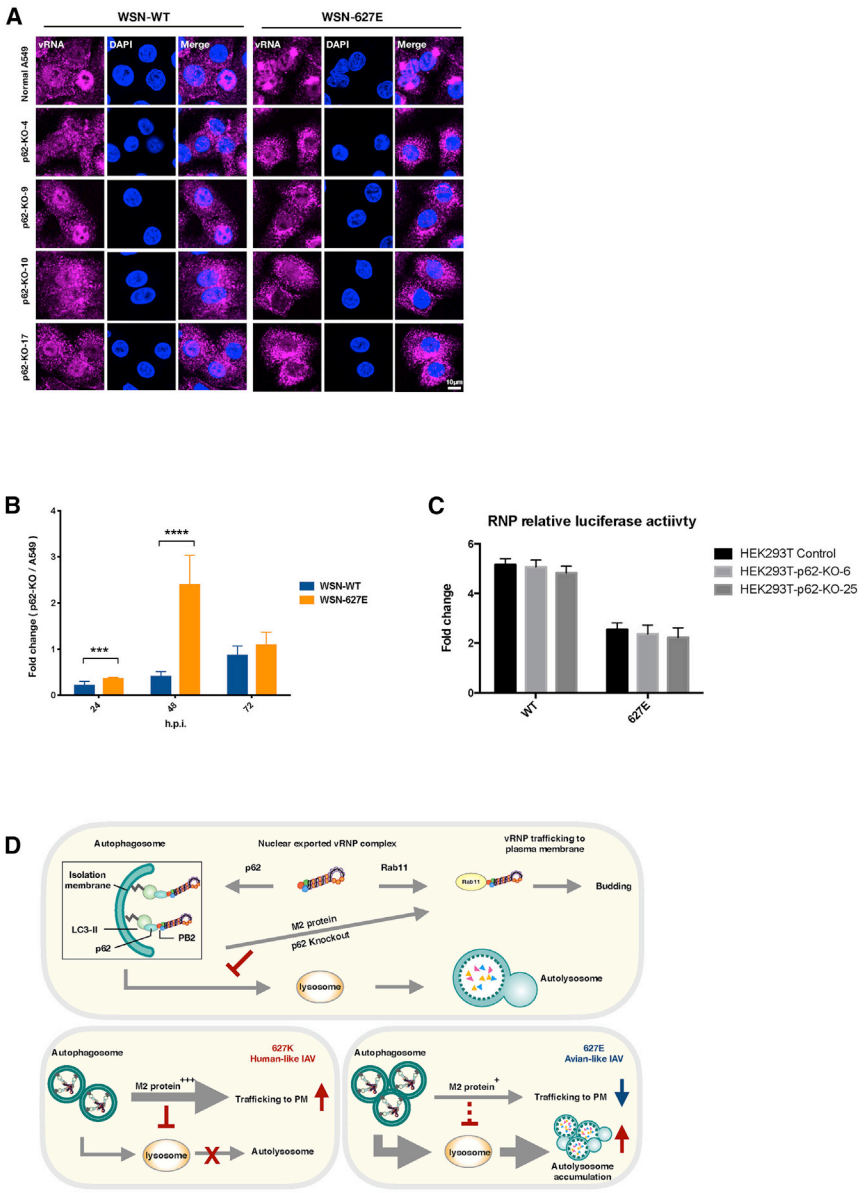

Figure 7. p62 is required for formation of vRNA aggregates in WSN-627E influenza virus-infected cells

(A) Different clones of p62-knockout A549 cells were infected with either WSN-WT or WSN-627E reassortant virus at an MOI of 5. Cells were fixed at 10 hpi and FISH staining for PB2 vRNA (purple) was performed. Merge images also include DAPI staining (blue). Images were acquired by confocal LSM 780 microscopy. Images are representative of 3 independent experiments. Scale bar, 10 μm.

(B) p62 KO or control A549 cells were infected with WSN-WT or WSN-627E viruses at an MOI of 0.001. Supernatants were collected at 24, 48, and 72 hpi and virus titers determined by plaque assay. Values represent the mean results of 3 separate experiments, and error bars represent SDs Statistical significance was analyzed by 1-way analysis of variance: ***$p < 0.001$ and ****$p < 0.0001$.

(C) RNP activity of WSN-WT and WSN-627E viruses in different p62 KO HEK293T clones. An RNP polymerase assay was conducted by co-transfecting pHW2000 plasmids containing NP, PB1, and PB2 from either WSN-627K or WSN-627E, together with a luciferase reporter plasmid and a thymidine kinase promoter-*Renilla* luciferase reporter plasmid (pRL_TK) construct. The luciferase activity was measured using a Dual-Luciferase Reporter Assay System (Promega) at 24 h post-transfection. RNP polymerase activity was normalized against pRL_TK activity. Data represent mean luciferase activity from 3 separate experiments, calculated after normalization with *Renilla* luciferase activity, ± SD.

(D) A working model for the interplay between virus adaptive strategies involving the influenza virus PB2 protein and intracellular trafficking, and involvement of the autophagy process following vRNP nuclear export in mammalian cells.

polymerase subunit, and influenza viruses containing PB2 with an adaptive mutation evade such restriction, possibly partly through optimal expression of the M2 protein, which blocks autophagosome fusion with lysosomes (Gannagé et al., 2009). We discovered that the p62 autophagy receptor interacts with PB2 and is crucial for this host-restriction process, as depletion of p62 prevents the formation of vRNP aggregates in cells infected with WSN-627E virus and enhances the replication of virus with avian-type PB2 (627E) virus more greatly than it does virus with mammalian-type PB2 (627K) (Figures 6C, 7A, and 7B). Therefore, the adaptive strategies of the influenza virus PB2 protein also involve evasion of host restriction of intracellular trafficking, besides the facilitation of nuclear import and optimization of viral polymerase activity in mammalian cells.

Host specificity prevents cross-species transmission of animal viruses, while evolution and environmental changes may drive viruses to expand their host range through the acquisition of host-adaptive mutations. Viruses use different adaptive strategies to evade host restriction. Influenza virus serves as an ideal model for studying virus host interactions because it is one of the few RNA viruses that infects multiple hosts and replicates in the nucleus of infected cells, providing opportunities for dissecting host barriers and virus-adaptive strategies throughout multiple stages of the virus life cycle. An excellent example is the multiple adaptive mutations acquired by different influenza viruses within the polymerase PB2 subunit, which optimize replication in mammalian cells (Soh et al., 2019; Song et al., 2014). Adaptive mutations in NP and other polymerase subunits also occur, as the viral polymerase functions as a complex (Chen et al., 2006a). It is hypothesized that this type of host adaptation may occur before species jumping, thereby priming the avian influenza virus to replicate sufficiently well in mammalian cells to allow the opportunity to

gain further adaptive mutations (Huang et al., 2017; Wang et al., 2019). Given the complicated replication process and life cycle of influenza A virus, there are multiple layers of host restriction targeting different stages of virus replication. For instance, RIG-I directly binds to incoming nucleocapsids, with enhanced specificity for PB2-627E RNP complexes, following the release of the viral genome from endosomes during influenza virus infection (Weber et al., 2015). Nuclear import is another barrier that determines the replication efficiency of influenza virus and is associated with PB2 host adaptation (Gabriel et al., 2008; Hudjetz and Gabriel, 2012). Upon entry to the nucleus, the influenza virus transcribes and replicates the viral genome using the viral polymerase complex. The effect of PB2 host adaptations on viral polymerase activity has been extensively studied, with the host factor ANP32A recently being found to act to restrict viral polymerase activity (Long et al., 2016). The present study further demonstrates that, after replication of the viral genome and nuclear export, host cells use restrictions through a mechanism involving the autophagic process to form vRNP aggregates, most likely leading to increased sequestration of unpackaged viral genomes and consequent limitation of virus replication efficiency. It is also possible that delays in intracellular trafficking caused by the formation of vRNP aggregates in the cytoplasm during the late stage of virion packaging may increase exposure to mediators of antiviral innate immunity in the cytosol, such as RIG-I, which further inhibits influenza virus replication efficiency.

Cross-talk between influenza virus infection-associated autophagy and apoptosis and modulation of these two cellular processes may determine virus replication efficiency. Harnessing the host response to infection through the activation of apoptosis may be critical for the successful replication of influenza virus. The current understanding is that in the early phase of replication, influenza virus suppresses apoptosis, most likely through the expression of NS1. In the late stage of infection, influenza virus hijacks the autophagy process though the function of the M2 protein to facilitate virus packaging (Gannagé et al., 2009). However, influenza viruses that have not gained host adaptations for replication in mammalian cells may not have acquired the full ability to interact with the cytoplasmic trafficking process, in addition to dealing with the other host-restricting barriers discussed above. Newly synthesized vRNA, which contains avian-type PB2 (e.g., PB2-627E) can be stalled by the impairment of cytoplasmic trafficking right after nuclear export, leading to the formation of vRNA aggregates in the perinuclear region of virus-infected cells. This assumption is supported by the observation through electron microscopy that autolysosomes formed at the MTOC (Figure 3D) and colocalization of vRNP aggregates and LC3B (Figure 3A). Autophagosomes formed in the cell periphery use the cytoskeletal protein dynein to move along microtubules to the cell center and subsequently cluster with juxtanuclear lysosomes (Kimura et al., 2008). This process appears to be consistent with our observations in cells infected with PB2-627E virus. Instead of reaching the virion packaging site, vRNPs of WSN-627E virus accumulate to form aggregates at the MTOC and tend to be targeted to autolysosomes for sequestration (Figures 3 and 4).

Autophagy is recognized as a host defense mechanism against viral infection, and studies suggest that selective autophagy to remove various cytosolic cargos, including pathogens, is mediated by the p62 autophagy receptor. The p62 protein is known to link ubiquitinated substrates and autophagosomes via its UBA domain (Rogov et al., 2014). However, p62 was also reported to play a role in ubiquitin-independent autophagic degradation of ALS (amyotrophic lateral sclerosis) mutant SOD1 through its interaction region (residues 178–224) rather than the UBA domain (Gal et al., 2009). Interestingly, our result showed that the region between the ZZ and TRAF6 domains of p62 (residues 163–225) is responsible for interaction with the viral PB2 protein and that p62 plays an important role in modulating the intracellular trafficking process of avian influenza virus vRNPs. Deletion of this region significantly impairs the interaction between p62 and PB2-627E and KO of p62 abolishes the formation of vRNA aggregates and enhances virus replication in A549 cells infected with PB2-627E virus (Figures 6, 7, and S6). It is important to note that the region of p62 spanned by residues 163–225 has been demonstrated to interact with Raptor, which is part of the mechanistic target of rapamycin complex 1 (mTORC1), with activated mTORC1 promoting autophagy (Duran et al., 2011). Our findings suggest an undefined relationship between p62 and influenza virus replication in which p62 interacts with PB2 in the viral polymerase complex through the region encompassed by residues 163–225 and competes with Raptor, leading to the inactivation of mTORC1 and promotion of the autophagy process (Figure S6B). However, it remains to be investigated how p62 mediates this process and whether other proteins are involved.

The M2 protein blocks autophagosome maturation and diverts LC3-conjugated membranes to the cell surface for budding of influenza viruses (Beale et al., 2014; Gannagé et al., 2009), showing that human influenza viruses have evolved with the ability to both evade and exploit host antiviral responses mediated through the autophagosome pathway. There are two possibilities that may independently or in combination lead to the formation of vRNP aggregates in avian-PB2 harboring virus infections: (1) avian influenza virus containing PB2-627E or other forms of avian PB2 fails to express sufficient M2 protein in mammalian cells to suppress the host antiviral process targeting the viral genome for degradation through the autophagic process; (2) the vRNP complexes of PB2-627E and PB2-627K viruses are differentially recognized by host machinery, and through antiviral activity of host factors more PB2-627E vRNP genomes are targeted to the autophagic process for autolysosomal sequestration. Our results suggest that the trafficking of vRNPs containing avian-type PB2 is disrupted and linked to the autolysosome, although we do not know whether degradation of these vRNP aggregates occurs. It has been previously shown that avian M genes are more frequently spliced into the M2 form, then accumulate in autophagosomes (Calderon et al., 2019). We show that influenza virus containing avian PB2 expresses lower levels of M2 protein and that ectopic expression of M2 blocks the formation of vRNA aggregates in avian-PB2 virus-infected mammalian cells, suggesting that viral proteins are suboptimally expressed from avian-PB2 viruses in these conditions (Figures 3 and 4). Viral polymerase complexes can regulate the choice of splice site for the expression of M RNAs (Shih et al., 1995). An adaptive mutation regulating the expression of NS1 and NEP mRNAs to facilitate virus replication in mammalian cells has

been identified in H7N9 virus (Huang et al., 2017). It remains to be determined whether avian-type and mammalian-type PB2 proteins influence influenza M mRNA splicing differently. We show that p62 is crucial for the formation of vRNP aggregates in cells infected with avian-type PB2 virus. Given that p62 is a key protein targeting substrates to autophagosomes through interaction with the region containing residues 163–225 and that deletion of this region impairs interaction between p62 and viral PB2, the role of p62 in influenza virus host adaptation warrants further study.

STAR★METHODS

Detailed methods are provided in the online version of this paper and include the following:

- KEY RESOURCES TABLE
- RESOURCE AVAILABILITY
  - Lead contact
  - Materials availability
  - Data and code availability
- EXPERIMENTAL MODEL AND SUBJECT DETAILS
- METHOD DETAILS
  - Reverse genetic (RG) influenza viruses and expression plasmids
  - Growth kinetic analysis of virus
  - Generation of knockout cell line with CRISPR/Cas9
  - Generation of GFP-RFP-LC3 stable expression cell lines
  - Transfection and protein expression
  - Co-immunoprecipitation (co-IP)
  - Luciferase assay
  - Combined immunofluorescence (IFA) and fluorescence *in situ* hybridization (FISH)
  - Flow cytometry
  - Transmission electron microscopy (TEM)
  - Quantitative real-time PCR
  - Cell viability assays
- QUANTIFICATION AND STATISTICAL ANALYSIS

SUPPLEMENTAL INFORMATION

Supplemental information can be found online at https://doi.org/10.1016/j.celrep.2021.109213.

ACKNOWLEDGMENTS

We thank Prof. Robert Webster for the pHW2000 plasmid. The authors are grateful to Dr. Jane Rayner for editing the manuscript. This study was supported in part by the Research Grants Council of the Hong Kong SAR (7629/13M, 17103214, 17154516, and 17107019) and the Health and Medical Research Fund (14131032).

AUTHOR CONTRIBUTIONS

H.C. and S.L. designed the studies; S.L., B.W.-Y.M., S.D., P.W., M.Z., S.-Y.L., P.C., X.H., H.L., C.J.C., Y.C., B.L., C.-Y.T., and W.S. performed the experiments; H.C., K.-Y.Y., and L.J. analyzed the data; and H.C. and S.L. wrote the paper.

DECLARATION OF INTERESTS

The authors declare no competing interests.

Received: December 9, 2020
Revised: April 7, 2021
Accepted: May 12, 2021
Published: June 8, 2021

REFERENCES

Amorim, M.J., Bruce, E.A., Read, E.K., Foeglein, A., Mahen, R., Stuart, A.D., and Digard, P. (2011). A Rab11- and microtubule-dependent mechanism for cytoplasmic transport of influenza A virus viral RNA. J. Virol. *85*, 4143–4156.

Beale, R., Wise, H., Stuart, A., Ravenhill, B.J., Digard, P., and Randow, F. (2014). A LC3-interacting motif in the influenza A virus M2 protein is required to subvert autophagy and maintain virion stability. Cell Host Microbe *15*, 239–247.

Bjørkøy, G., Lamark, T., Brech, A., Outzen, H., Perander, M., Overvatn, A., Stenmark, H., and Johansen, T. (2005). p62/SQSTM1 forms protein aggregates degraded by autophagy and has a protective effect on huntingtin-induced cell death. J. Cell Biol. *171*, 603–614.

Boivin, S., and Hart, D.J. (2011). Interaction of the influenza A virus polymerase PB2 C-terminal region with importin alpha isoforms provides insights into host adaptation and polymerase assembly. J. Biol. Chem. *286*, 10439–10448.

Calderon, B.M., Danzy, S., Delima, G.K., Jacobs, N.T., Ganti, K., Hockman, M.R., Conn, G.L., Lowen, A.C., and Steel, J. (2019). Dysregulation of M segment gene expression contributes to influenza A virus host restriction. PLoS Pathog. *15*, e1007892.

Cauldwell, A.V., Long, J.S., Moncorgé, O., and Barclay, W.S. (2014). Viral determinants of influenza A virus host range. J. Gen. Virol. *95*, 1193–1210.

Chen, D., and Zhong, Q. (2012). A tethering coherent protein in autophagosome maturation. Autophagy *8*, 985–986.

Chen, G.W., Chang, S.C., Mok, C.K., Lo, Y.L., Kung, Y.N., Huang, J.H., Shih, Y.H., Wang, J.Y., Chiang, C., Chen, C.J., and Shih, S.R. (2006a). Genomic signatures of human versus avian influenza A viruses. Emerg. Infect. Dis. *12*, 1353–1360.

Chen, H., Smith, G.J., Li, K.S., Wang, J., Fan, X.H., Rayner, J.M., Vijaykrishna, D., Zhang, J.X., Zhang, L.J., Guo, C.T., et al. (2006b). Establishment of multiple sublineages of H5N1 influenza virus in Asia: implications for pandemic control. Proc. Natl. Acad. Sci. USA *103*, 2845–2850.

Chen, Y., Liang, W., Yang, S., Wu, N., Gao, H., Sheng, J., Yao, H., Wo, J., Fang, Q., Cui, D., et al. (2013). Human infections with the emerging avian influenza A H7N9 virus from wet market poultry: clinical analysis and characterisation of viral genome. Lancet *381*, 1916–1925.

De Brabander, M.J., Van de Veire, R.M., Aerts, F.E., Borgers, M., and Janssen, P.A. (1976). The effects of methyl (5-(2-thienylcarbonyl)-1H-benzimidazol-2-yl) carbamate, (R 17934; NSC 238159), a new synthetic antitumoral drug interfering with microtubules, on mammalian cells cultured in vitro. Cancer Res. *36*, 905–916.

de Castro Martin, I.F., Fournier, G., Sachse, M., Pizarro-Cerda, J., Risco, C., and Naffakh, N. (2017). Influenza virus genome reaches the plasma membrane via a modified endoplasmic reticulum and Rab11-dependent vesicles. Nat. Commun. *8*, 1396.

de Graaf, M., and Fouchier, R.A. (2014). Role of receptor binding specificity in influenza A virus transmission and pathogenesis. EMBO J. *33*, 823–841.

Ding, B., Zhang, G., Yang, X., Zhang, S., Chen, L., Yan, Q., Xu, M., Banerjee, A.K., and Chen, M. (2014). Phosphoprotein of human parainfluenza virus type 3 blocks autophagosome-lysosome fusion to increase virus production. Cell Host Microbe *15*, 564–577.

Domingues, P., and Hale, B.G. (2017). Functional Insights into ANP32A-Dependent Influenza A Virus Polymerase Host Restriction. Cell Rep. *20*, 2538–2546.

Duran, A., Amanchy, R., Linares, J.F., Joshi, J., Abu-Baker, S., Porollo, A., Hansen, M., Moscat, J., and Diaz-Meco, M.T. (2011). p62 is a key regulator of nutrient sensing in the mTORC1 pathway. Mol. Cell *44*, 134–146.

Eisfeld, A.J., Kawakami, E., Watanabe, T., Neumann, G., and Kawaoka, Y. (2011). RAB11A is essential for transport of the influenza virus genome to the plasma membrane. J. Virol. *85*, 6117–6126.

Eskelinen, E.L. (2008). New insights into the mechanisms of macroautophagy in mammalian cells. Int. Rev. Cell Mol. Biol. *266*, 207–247.

Gabriel, G., Dauber, B., Wolff, T., Planz, O., Klenk, H.D., and Stech, J. (2005). The viral polymerase mediates adaptation of an avian influenza virus to a mammalian host. Proc. Natl. Acad. Sci. USA *102*, 18590–18595.

Gabriel, G., Herwig, A., and Klenk, H.D. (2008). Interaction of polymerase subunit PB2 and NP with importin alpha1 is a determinant of host range of influenza A virus. PLoS Pathog. *4*, e11.

Gal, J., Ström, A.L., Kwinter, D.M., Kilty, R., Zhang, J., Shi, P., Fu, W., Wooten, M.W., and Zhu, H. (2009). Sequestosome 1/p62 links familial ALS mutant SOD1 to LC3 via an ubiquitin-independent mechanism. J. Neurochem. *111*, 1062–1073.

Gannagé, M., Dormann, D., Albrecht, R., Dengjel, J., Torossi, T., Rämer, P.C., Lee, M., Strowig, T., Arrey, F., Conenello, G., et al. (2009). Matrix protein 2 of influenza A virus blocks autophagosome fusion with lysosomes. Cell Host Microbe *6*, 367–380.

Gao, R., Cao, B., Hu, Y., Feng, Z., Wang, D., Hu, W., Chen, J., Jie, Z., Qiu, H., Xu, K., et al. (2013). Human infection with a novel avian-origin influenza A (H7N9) virus. N. Engl. J. Med. *368*, 1888–1897.

Guichard, A., Nizet, V., and Bier, E. (2014). RAB11-mediated trafficking in host-pathogen interactions. Nat. Rev. Microbiol. *12*, 624–634.

Hatta, M., Gao, P., Halfmann, P., and Kawaoka, Y. (2001). Molecular basis for high virulence of Hong Kong H5N1 influenza A viruses. Science *293*, 1840–1842.

Huang, X., Zheng, M., Wang, P., Mok, B.W., Liu, S., Lau, S.Y., Chen, P., Liu, Y.C., Liu, H., Chen, Y., et al. (2017). An NS-segment exonic splicing enhancer regulates influenza A virus replication in mammalian cells. Nat. Commun. *8*, 14751.

Hudjetz, B., and Gabriel, G. (2012). Human-like PB2 627K influenza virus polymerase activity is regulated by importin-α1 and -α7. PLoS Pathog. *8*, e1002488.

Hutchinson, E.C., Charles, P.D., Hester, S.S., Thomas, B., Trudgian, D., Martínez-Alonso, M., and Fodor, E. (2014). Conserved and host-specific features of influenza virion architecture. Nat. Commun. *5*, 4816.

Johnston, J.A., Ward, C.L., and Kopito, R.R. (1998). Aggresomes: a cellular response to misfolded proteins. J. Cell Biol. *143*, 1883–1898.

Kabeya, Y., Mizushima, N., Ueno, T., Yamamoto, A., Kirisako, T., Noda, T., Kominami, E., Ohsumi, Y., and Yoshimori, T. (2000). LC3, a mammalian homologue of yeast Apg8p, is localized in autophagosome membranes after processing. EMBO J. *19*, 5720–5728.

Kabeya, Y., Mizushima, N., Yamamoto, A., Oshitani-Okamoto, S., Ohsumi, Y., and Yoshimori, T. (2004). LC3, GABARAP and GATE16 localize to autophagosomal membrane depending on form-II formation. J. Cell Sci. *117*, 2805–2812.

Katsuragi, Y., Ichimura, Y., and Komatsu, M. (2015). p62/SQSTM1 functions as a signaling hub and an autophagy adaptor. FEBS J. *282*, 4672–4678.

Kimura, S., Noda, T., and Yoshimori, T. (2007). Dissection of the autophagosome maturation process by a novel reporter protein, tandem fluorescent-tagged LC3. Autophagy *3*, 452–460.

Kimura, S., Noda, T., and Yoshimori, T. (2008). Dynein-dependent movement of autophagosomes mediates efficient encounters with lysosomes. Cell Struct. Funct. *33*, 109–122.

Komatsu, M., Kurokawa, H., Waguri, S., Taguchi, K., Kobayashi, A., Ichimura, Y., Sou, Y.S., Ueno, I., Sakamoto, A., Tong, K.I., et al. (2010). The selective autophagy substrate p62 activates the stress responsive transcription factor Nrf2 through inactivation of Keap1. Nat. Cell Biol. *12*, 213–223.

Kuo, S.M., Chen, C.J., Chang, S.C., Liu, T.J., Chen, Y.H., Huang, S.Y., and Shih, S.R. (2017). Inhibition of Avian Influenza A Virus Replication in Human Cells by Host Restriction Factor TUFM Is Correlated with Autophagy. MBio *8*, e00481-17.

Labadie, K., Dos Santos Afonso, E., Rameix-Welti, M.A., van der Werf, S., and Naffakh, N. (2007). Host-range determinants on the PB2 protein of influenza A viruses control the interaction between the viral polymerase and nucleoprotein in human cells. Virology *362*, 271–282.

Lakdawala, S.S., Fodor, E., and Subbarao, K. (2016). Moving On Out: Transport and Packaging of Influenza Viral RNA into Virions. Annu. Rev. Virol. *3*, 411–427.

Lamb, R.A., and Krug, R.M. (2001). Orthomyxoviridae: The Viruses and Their Replication. In Fundamental Virology, Fourth Edition, D.M. Knipe and P.M. Howley, eds. (Lippincott Williams & Wilkins), pp. 725–769.

Levine, B. (2005). Eating oneself and uninvited guests: autophagy-related pathways in cellular defense. Cell *120*, 159–162.

Long, J.S., Giotis, E.S., Moncorgé, O., Frise, R., Mistry, B., James, J., Morisson, M., Iqbal, M., Vignal, A., Skinner, M.A., and Barclay, W.S. (2016). Species difference in ANP32A underlies influenza A virus polymerase host restriction. Nature *529*, 101–104.

Long, J.S., Idoko-Akoh, A., Mistry, B., Goldhill, D., Staller, E., Schreyer, J., Ross, C., Goodbourn, S., Shelton, H., Skinner, M.A., et al. (2019). Species specific differences in use of ANP32 proteins by influenza A virus. eLife *8*, e45066.

Mänz, B., Brunotte, L., Reuther, P., and Schwemmle, M. (2012). Adaptive mutations in NEP compensate for defective H5N1 RNA replication in cultured human cells. Nat. Commun. *3*, 802.

Mehle, A., and Doudna, J.A. (2009). Adaptive strategies of the influenza virus polymerase for replication in humans. Proc. Natl. Acad. Sci. USA *106*, 21312–21316.

Mizushima, N., Yoshimori, T., and Levine, B. (2010). Methods in mammalian autophagy research. Cell *140*, 313–326.

Momose, F., Kikuchi, Y., Komase, K., and Morikawa, Y. (2007). Visualization of microtubule-mediated transport of influenza viral progeny ribonucleoprotein. Microbes Infect. *9*, 1422–1433.

Naffakh, N., Tomoiu, A., Rameix-Welti, M.A., and van der Werf, S. (2008). Host restriction of avian influenza viruses at the level of the ribonucleoproteins. Annu. Rev. Microbiol. *62*, 403–424.

Naviaux, R.K., Costanzi, E., Haas, M., and Verma, I.M. (1996). The pCL vector system: rapid production of helper-free, high-titer, recombinant retroviruses. J. Virol. *70*, 5701–5705.

Ogrodnik, M., Salmonowicz, H., Brown, R., Turkowska, J., Średniawa, W., Pattabiraman, S., Amen, T., Abraham, A.C., Eichler, N., Lyakhovetsky, R., and Kaganovich, D. (2014). Dynamic JUNQ inclusion bodies are asymmetrically inherited in mammalian cell lines through the asymmetric partitioning of vimentin. Proc. Natl. Acad. Sci. USA *111*, 8049–8054.

Pankiv, S., Clausen, T.H., Lamark, T., Brech, A., Bruun, J.A., Outzen, H., Øvervatn, A., Bjørkøy, G., and Johansen, T. (2007). p62/SQSTM1 binds directly to Atg8/LC3 to facilitate degradation of ubiquitinated protein aggregates by autophagy. J. Biol. Chem. *282*, 24131–24145.

Pumroy, R.A., Ke, S., Hart, D.J., Zachariae, U., and Cingolani, G. (2015). Molecular determinants for nuclear import of influenza A PB2 by importin α isoforms 3 and 7. Structure *23*, 374–384.

Ran, F.A., Hsu, P.D., Wright, J., Agarwala, V., Scott, D.A., and Zhang, F. (2013). Genome engineering using the CRISPR-Cas9 system. Nat. Protoc. *8*, 2281–2308.

Rogov, V., Dötsch, V., Johansen, T., and Kirkin, V. (2014). Interactions between autophagy receptors and ubiquitin-like proteins form the molecular basis for selective autophagy. Mol. Cell *53*, 167–178.

Rujano, M.A., Bosveld, F., Salomons, F.A., Dijk, F., van Waarde, M.A., van der Want, J.J., de Vos, R.A., Brunt, E.R., Sibon, O.C., and Kampinga, H.H. (2006). Polarised asymmetric inheritance of accumulated protein damage in higher eukaryotes. PLoS Biol. *4*, e417.

Schrauwen, E.J., and Fouchier, R.A. (2014). Host adaptation and transmission of influenza A viruses in mammals. Emerg. Microbes Infect. *3*, e9.

Shih, S.R., Nemeroff, M.E., and Krug, R.M. (1995). The choice of alternative 5′ splice sites in influenza virus M1 mRNA is regulated by the viral polymerase complex. Proc. Natl. Acad. Sci. USA *92*, 6324–6328.

Soh, Y.S., Moncla, L.H., Eguia, R., Bedford, T., and Bloom, J.D. (2019). Comprehensive mapping of adaptation of the avian influenza polymerase protein PB2 to humans. eLife *8*, e45079.

Song, W., Wang, P., Mok, B.W., Lau, S.Y., Huang, X., Wu, W.L., Zheng, M., Wen, X., Yang, S., Chen, Y., et al. (2014). The K526R substitution in viral protein PB2 enhances the effects of E627K on influenza virus replication. Nat. Commun. *5*, 5509.

Subbarao, E.K., London, W., and Murphy, B.R. (1993). A single amino acid in the PB2 gene of influenza A virus is a determinant of host range. J. Virol. *67*, 1761–1764.

Taubenberger, J.K., and Kash, J.C. (2010). Influenza virus evolution, host adaptation, and pandemic formation. Cell Host Microbe *7*, 440–451.

Wang, X., Jiang, H., Wu, P., Uyeki, T.M., Feng, L., Lai, S., Wang, L., Huo, X., Xu, K., Chen, E., et al. (2017). Epidemiology of avian influenza A H7N9 virus in human beings across five epidemics in mainland China, 2013-17: an epidemiological study of laboratory-confirmed case series. Lancet Infect. Dis. *17*, 822–832.

Wang, P., Song, W., Mok, B.W., Zheng, M., Lau, S.Y., Liu, S., Chen, P., Huang, X., Liu, H., Cremin, C.J., and Chen, H. (2019). The PB2 Polymerase Host Adaptation Substitutions Prime Avian Indonesia Sub Clade 2.1 H5N1 Viruses for Infecting Humans. Viruses *11*, 292.

Weber, M., Sediri, H., Felgenhauer, U., Binzen, I., Bänfer, S., Jacob, R., Brunotte, L., García-Sastre, A., Schmid-Burgk, J.L., Schmidt, T., et al. (2015). Influenza virus adaptation PB2-627K modulates nucleocapsid inhibition by the pathogen sensor RIG-I. Cell Host Microbe *17*, 309–319.

Yamada, S., Hatta, M., Staker, B.L., Watanabe, S., Imai, M., Shinya, K., Sakai-Tagawa, Y., Ito, M., Ozawa, M., Watanabe, T., et al. (2010). Biological and structural characterization of a host-adapting amino acid in influenza virus. PLoS Pathog. *6*, e1001034.

Yeganeh, B., Ghavami, S., Rahim, M.N., Klonisch, T., Halayko, A.J., and Coombs, K.M. (2018). Autophagy activation is required for influenza A virus-induced apoptosis and replication. Biochim. Biophys. Acta Mol. Cell Res. *1865*, 364–378.

Zheng, M., Wang, P., Song, W., Lau, S.Y., Liu, S., Huang, X., Mok, B.W., Liu, Y.C., Chen, Y., Yuen, K.Y., and Chen, H. (2015). An A14U Substitution in the 3′ Noncoding Region of the M Segment of Viral RNA Supports Replication of Influenza Virus with an NS1 Deletion by Modulating Alternative Splicing of M Segment mRNAs. J. Virol. *89*, 10273–10285.

STAR★METHODS

KEY RESOURCES TABLE

REAGENT or RESOURCE	SOURCE	IDENTIFIER
Antibodies		
Mouse monoclonal antibody anti-Influenza A NS1	Dr Yee-Joo Tan (NUS)	N/A
Mouse polyclonal antibody anti-Influenza A PB2	Laboratory-made (Song et al., 2014)	N/A
Mouse polyclonal antibody anti-Influenza A PB1	Laboratory-made (Song et al., 2014)	N/A
Mouse polyclonal antibody anti-Influenza A PA	Laboratory-made (Song et al., 2014)	N/A
Mouse polyclonal antibody anti-Influenza A NP	Laboratory-made (Song et al., 2014)	N/A
Rabbit monoclonal anti-APG5L/Atg5	Abcam	Cat# ab108327, RRID:AB_2650499
Rabbit monoclonal anti-Rab11(D4F5)	Cell Signaling Technology	Cat# 5589, RRID:AB_10693925
Mouse monoclonal anti-Influenza A m1(FluAc)	Santa Cruz Biotechnology	Cat# sc-69824, RRID:AB_1124287
Mouse monoclonal anti-Influenza A m2(14C2)	Abcam	Cat# ab5416, RRID:AB_304873
Rabbit polyclonal anti-Influenza A NS2/NEP	GenScript	Cat# A01499, RRID:AB_1968849
Rabbit monoclonal anti-Vimentin	Abcam	Cat# ab92547, RRID:AB_10562134
Mouse monoclonal anti-alpha Tubulin	Abcam	Cat# ab7291, RRID:AB_2241126
Rabbit polyclonal anti-LC3B	Sigma-Aldrich	Cat# L7543, RRID:AB_796155
Mouse monoclonal anti-SQSTM1/p62 (D-3)	Santa Cruz Biotechnology	Cat# sc-28359, RRID:AB_628279
Rabbit monoclonal anti-SQSTM1/p62	Abcam	Cat# ab109012, RRID:AB_2810880
Mouse monoclonal anti-Flag(M2)	Sigma-Aldrich	Cat# P2983, RRID:AB_439685
Rabbit monoclonal anti-Flag (SIG-25)	Sigma-Aldrich	Cat# F2555, RRID:AB_796202
Mouse monoclonal anti- beta Actin	Abcam	Cat# ab8226, RRID:AB_306371
Rabbit monoclonal anti-GM130	Abcam	Cat# ab52649, RRID:AB_880266
Rabbit monoclonal anti-TGN46	Abcam	Cat# ab174280, RRID:N/A
Rabibit monoclonal anti-Calnexin	Abcam	Cat# ab133615, RRID:AB_2864299
Rabbit monoclonal anti-LAMP1 (D2D11)	Cell Signaling Technology	Cat# 9091, RRID:AB_2687579
Mouse monoclonal anti-Optineurin/ OPTN(C-2)	Santa Cruz Biotechnology	Cat# sc-166576, RRID:AB_2156554
Rabbit polyclonal anti-TUFM	Thermo Fisher Scientific	Cat# PA5-27511, RRID:AB_2544987
Rabbit polyclonal anti-RIG-I/DDX58	Abclonal	Cat# A0550, RRID:AB_2757259
Mouse monoclonal anti-Ub proteins (FK2)	Millipore	Cat# 04-263, RRID:AB_612093
Rabbit polyclonal anti-actin	Abcam	Cat# ab8227, RRID:AB_2305186
Bacterial and virus strains		
A/Zhejiang/DTID-ZJU01/2013 (Human H7N9)	Isolated (Song et al., 2014)	N/A
A/CK/Zhejiang/DTID-ZJU01/2013 (Avian H7N9)	Isolated (Song et al., 2014)	N/A
A/HK/3239/2008 (H9N2)	Isolated (Song et al., 2014)	N/A
Chemicals		
Nocodazole	Cell Signaling Technology	Cat# 2190
Bafilomycin A1	Invivogen	Cat# tlrl-baf1

(*Continued on next page*)

Continued

REAGENT or RESOURCE	SOURCE	IDENTIFIER
Experimental models: Cell lines		
Human lung carcinoma cell line A549	ATCC	Cat# CCL-185
Human embryonic kidney cell line HEK293T	ATCC	Cat# CRL-11268
Mouse Embryonic Fibroblast MEF	ATCC	Cat# CRL-2907
Madin-Darby Canine Kidney MDCK	ATCC	Cat# CCL-34
Chicken embryonic fibroblast cell line DF-1	ATCC	Cat# CRL-12203
Primary normal human bronchial epithelial (NHBE)	Lonza	N/A
A549-p62-KO	This paper	N/A
293T-p62-KO	This paper	N/A
Oligonucleotides		
Primers for Human GAPDH Forward: AAGGTCATCCCAGAGCTGAA	This paper	N/A
Primers for Human GAPDH Reverse: CTGCTTCACCACCTTCTTGA	This paper	N/A
Primers for Human IFIT1 Forward: GCCTTGCTGAAGTGTGGAGGAA	This paper	N/A
Primers for Human IFIT1 Reverse: ATCCAGGCGATAGGCAGAGATC	This paper	N/A
Primers for Human p62 gene KO Forward: CACCGCGACTTGTGTAGCGTCTGCG	This paper	N/A
Primers for Human p62 gene KO Reverse: AAACCGCAGACGCTACACAAGTCGC	This paper	N/A
Primers for p62-Flag clone Forward: ATGGCGTCGCTCACCGTGAAGGCC	This paper	N/A
Primers for p62-Flag clone Reverse: TCACAACGGCGGGGGATGCTTTGAA	This paper	N/A
Recombinant DNA		
pHW2000-PB2-N-Flag	This paper	N/A
pEF-N-V5-M2	This paper	N/A
pcDNA3.1-p62	This paper	N/A
pX459 CRISPR/Cas9-Puro vector	Laboratory of Feng Zhang	Addgene # 48139; RRID: Addgene_48139
pX459-p62	This paper	N/A
pcl-Eco	Laboratory of Inder Verma	Addgene # 12371; RRID: Addgene_12371
ptfLC3	Laboratory of Tamotsu Yoshimori	Addgene # 21074; RRID: Addgene_21074
Software and algorithms		
GraphPad Prism 8	GraphPad	N/A
ZEISS ZEN imaging Software	ZEISS	N/A
ImageJ	ImageJ	N/A

RESOURCE AVAILABILITY

Lead contact

Further information and requests for resources and reagents should be directed to and will be fulfilled by the Lead Contact, Honglin Chen (hlchen@hku.hk)

Materials availability

All new reagents are available by Materials Transfer Agreement for non-commercial research.

Data and code availability

This study did not generate any unique datasets or code.

EXPERIMENTAL MODEL AND SUBJECT DETAILS

Human lung carcinoma cell line A549 (ATCC), human embryonic kidney cell line HEK293T (ATCC), Mouse Embryonic Fibroblast (MEF-ATCC), Madin-Darby Canine Kidney (MDCK-ATCC) and chicken embryonic fibroblast cell line DF-1 (ATCC) cells were cultured at 37°C in Dulbecco's Modified Eagle Medium (DMEM) (Thermo Fisher Scientific) supplemented with 10% FBS and 1% Penicillin/Streptomycin (P/S) and maintained in a 5% CO_2 atmosphere. Primary normal human bronchial epithelial (NHBE) cells derived from human tracheal/bronchial tissues were purchased from Lonza. Cells were grown in serum-free growth factor-supplemented medium and cultured to form a confluent monolayer for subsequent infection experiments.

METHOD DETAILS

Reverse genetic (RG) influenza viruses and expression plasmids

The reverse genetic influenza virus strains A/WSN/1933 (H1N1) (WSN), A/Zhejiang/DTID-ZJU01/2013 (human H7N9), A/CK/Zhejiang/DTID-ZJU01/2013 (avian H7N9) and A/HK/3239/2008 (H9N2) are as previously described (Huang et al., 2017; Song et al., 2014; Zheng et al., 2015). Flag tagged pHW2000-PB2-N-Flag (WT or 627E) plasmids and those for expressing different PB2 mutants, including K526R, K526R/E627K, E627K, K627E, Q591K and D701N were constructed using the QuikChange site-directed mutagenesis kit (Agilent) according to the standard protocol and used for rescue of reverse genetic versions of viruses using the WSN backbone with a previously described protocol (Zheng et al., 2015). The M2 gene from the WSN strain was cloned into the pEF-N-V5 vector. Full length p62 and various truncated forms were cloned into the pcDNA3.1 vector.

Growth kinetic analysis of virus

Confluent A549, DF-1, p62 knockout A549 or RIG-I knockout A549 cells seeded in 48-well plates were washed with PBS once and infected with diluted virus at the indicated multiplicity of infection (MOI). After 1 h adsorption, supernatant was removed, and infected cells were washed twice with PBS, and then cultured in MEM medium containing 0.1% TPCK-treated trypsin at 37°C. Supernatants were collected at the indicated time points by centrifugation at 13000 x g for 1 m to remove dead cells and stored at −80°C until being titrated. Virus titers were determined by plaque assay in MDCK cells.

Generation of knockout cell line with CRISPR/Cas9

To knockout human p62, guide RNA 5′-CACCGCCAGGCGCACTACCGCGATG-3′/5′-AAACCATCGCGGTAGTGCGCCTGGC-3′ was designed for CRISPR/Cas9 by using the GenScript gRNA database. Annealed complementary oligonucleotides for guide RNAs (gRNAs) were cloned into the pX459 CRISPR/Cas9-Puro vector (Addgene)(Ran et al., 2013). HEK293T cells and A549 cells were transfected with pX459/gRNA using TransLT-1 (Mirus), according to the manufacturer's instructions. After two days cells were treated with different concentrations of puromycin (8 μg/ml for HEK293T and 2 μg/ml for A549) for two days. Colonies were isolated after two weeks, and the p62 sequences then analyzed and protein expression detected by western blot.

Generation of GFP-RFP-LC3 stable expression cell lines

To generate GFP-RFP-LC3 stable cell lines, a retroviral vector was used to deliver heritable genes into the genome of target cells. Briefly, one 10cm dish of 293FT cells with 50% confluency were co-transfected with pcl-Eco (ecotropic receptor for mouse cell line) or pcl-Ampho (amphotropic receptor for human cell line) and mCherry-EGFP-LC3 plasmids (Naviaux et al., 1996). The supernatant was harvested 48 h after transfection and centrifuged at 3000 x g for 3 m at 4°C to remove cell debris. Supernatant was filtered through a 0.45 μm syringe filter and retrovirus subsequently concentrated using PEG-*it* (SBI #LV825A-1) according to the manufacturer's manual at 4°C overnight. MEF or A549 cells cultured in a 6-well plate were transduced with retrovirus and incubated at 37°C. After 48 h, puromycin (1:5000) was added into the medium for selection of positive cells.

Transfection and protein expression

Trans-LT-1 was used to transfect plasmids into HEK293T cells growing at 70%–80% confluency. For plasmid transfection in a 6-well plate, 2000ng of plasmid DNA was added into a mixture of 200 μL of OPTI-MEM and 7.5 μL of Trans-LT-1 reagent. The mixture was then gently pipetted to mix and kept at room temperature for 30 m before being added onto the cells. The amount of plasmid and the volume of OPTI-MEM and transfection reagent for 10cm dishes or 12-well plates was scaled up or down as needed. For protein overexpression, HEK293T cells were transfected for 36-48 h before harvest. A549 cells were also transfected using Trans-LT-1 reagent for immunofluorescence assay (IFA) experiments, despite a low transfection efficiency.

Co-immunoprecipitation (co-IP)

HEK293T and p62 KO HEK293T cells were seeded at 70%–80% confluency into 10cm dishes and then co-transfected with protein expression plasmids. After 36-48 h, cells were collected and washed twice with cold PBS by centrifugation at 500 x g for 5 m. Subsequently, cell pellets were lysed in 1ml lysis buffer (50mM Tris HCl, pH 7.4, 150mM NaCl, 1mM EDTA, 1% Triton X-100 with protease inhibitor cocktail (Roche), and the DUB inhibitor 1,10-phenanthroline monohydrate (P9375; Sigma), as needed) on ice for 30 m and centrifuged at 16000 x g for 10 m at 4°C to remove cell debris. 10% of the supernatant was retained as INPUT and the remainder was used for co-IP. For the standard immunoprecipitation assay, 50 μL of Dynabeads (Thermo Fisher Scientific) were washed three times

with 500 μL of lysis buffer. Specific antibody or control IgG antibody was then added to the beads, followed by mixing at room temperature for 30 m. After washing with lysis buffer, beads were evenly distributed into lysates. For co-IP using Anti-FLAG® M2 Magnetic Beads (Sigma), beads were washed with lysis buffer and added directly into lysates. After incubation at 4°C overnight, beads were washed five times with 500 μL of lysis buffer, resuspended in SDS sample buffer and boiled at 95°C for 10 m.

Luciferase assay

To compare the polymerase activity of RNP complexes in different cell lines, dual luciferase activity reporter assays were performed. RNP complex expression plasmids composed of PB2 (WT or 627E), PB1, PA and NP (50ng each), together with pYH-Luci reporter plasmid (30ng) and Renilla reporter plasmid (10ng) were co-transfected into HEK293T cells. At 24 h after transfection, cells were lysed and the luciferase activity was measured using the Dual-Luciferase reporter assay system (Promega).

Combined immunofluorescence (IFA) and fluorescence *in situ* hybridization (FISH)

A549 or NHBE cells in 8-well Millicell EZ slides (Millipore) were infected with the indicated viruses and harvested at various time points. After fixation with 4% paraformaldehyde (PFA) at room temperature for 30 m, cells were washed twice with PBS and permeabilized in 70% ethanol overnight. After discarding the ethanol and washing twice with FISH washing buffer (10% 20X SSC, 10% formamide in water), cells were incubated in FISH buffer (10% formamide, 10% dextran sulfate and 10% 20X SSC in water) with Stellaris® RNA probes for specific vRNA or mRNA (1:100, Biosearch Technologies Company) and up to two different primary antibodies (1:100-200) at 37°C for 5 h. Slides were then washed twice with FISH washing buffer and incubated with the corresponding secondary antibodies at room temperature for 1 h. After washing with FISH washing buffer three times, slides were mounted using mounting buffer containing DAPI (VECTASHIELD). Images were acquired using an LSM710 or LSM780 confocal microscope (Leica Microsystems) and ZEN software used for analysis.

Flow cytometry

Confluent cultures of the wild-type MEF cell line stably expressing mRFP/mCherry-EGFP-LC3, generated by retrovirus infection, were infected with WSN-WT or WSN-627E. After infection, cells were washed with PBS and detached from the culture vessel by incubation with 0.05% trypsin-EDTA at 37°C for 3 m. Cells were resuspended in DMEM containing 10% FBS, then transferred to a new 1.5ml Eppendorf tube for centrifugation at 500 x g for 5 m at 4°C. Cells were then washed twice with cold PBS and fixed on ice with 2% PFA. After 30 m, cells were analyzed on a BD LSRFortessa Analyzer (BD Life Sciences) with detection of FITC (530/30nm) and PE/PI (585/42nm). Twenty thousand events for each sample were acquired, with each measurement being repeated three times. FlowJo software was used to analyze the acquired data.

Transmission electron microscopy (TEM)

For high pressure freezing (HPF), A549 cells which had undergone the indicated treatments were pelleted, resuspended in 20% BSA in DMEM with cryo-protector and immediately high-pressure frozen in a high-pressure freezer (EM PACT2, Leica), followed by subsequent freeze substitution in acetone containing 0.4% uranyl acetate at −85°C in an AFS freeze-substitution unit. After gradient infiltration with an increasing concentration of HM20 in pure ethanol, samples were embedded and ultraviolet polymerized for ultra-thin sectioning and imaging. TEM examination was done with a Hitachi H-7650 transmission electron microscope with a charge-coupled device camera operating at 80 kV (Hitachi High-Technologies Corporation).

Quantitative real-time PCR

Total RNAs were extracted from cells using RNAzol (Molecular Research Center) according to the manufacturer's manual. Extracted RNAs were reverse transcribed into complementary DNAs (cDNAs) using a PrimeScript RT Reagent Kit (Takara) in accordance with the user manual. For viral and host mRNA detection, oligo-dT was used as the primer. Complementary DNAs were diluted 20-fold in ultra-pure water before being subjected to quantitative real-time PCR (RT-qPCR), performed on a LightCycler 480 instrument (Roche) using the SYBR Premix Ex Taq Kit (Takara). Relative mRNA expression was measured using the ΔΔCT method and Delta-deltacycle values were normalized to the average expression of GAPDH to calculate host and viral gene expression.

Cell viability assays

Cellular cytotoxicity was assessed using a CCK8 assay kit (MedChemExpress: HY-K0301). A549 cells in a 96-well plate were infected either with WSN-WT or WSN-627E viruses, or mock infected. At the indicated time points, 10 μL of CCK8 solution was added into each well, followed by an additional incubation at 37°C for 3 hours. The absorbance at 450nm was then measured in a Varioskan LUX multimode micro-plate reader (Thermo Fisher Scientific). All assays were performed in biologically independent triplicate.

QUANTIFICATION AND STATISTICAL ANALYSIS

All the statistical analyses have been performed using Prism 8 Graph Pad Software. The significance of differences between two or three experimental groups (cells infected with the control, WSN-WT and WSN-627E) was determined by the Student t test. All data are presented as means ± s.d. Statistical significance was analyzed by one-way analysis of variance: ****$p < 0.0001$, ***$p < 0.001$, **$p < 0.01$, *$p < 0.05$ and ns = not significant.